MODELING, SIMULATION, AND MONITORING OF A PHOTOVOLTAIC

APPLICATION POWERING A FLYHWEEL ENERGY STORAGE SYSTEM

A Thesis

by

MOHAMED TAREK MOHAMED HUSSEIN MOHAMED

Submitted to the Office of Graduate and Professional Studies of
Texas A&M University
in partial fulfillment of the requirements for the degree of

MASTER OF SCIENCE

Chair of Committee,	Reza Tafreshi
Co-Chair of Committee,	Alan Palazzolo
Committee Member,	Mohammad Naraghi
Head of Department,	Andreas Polycarpou

December 2019

Major Subject: Mechanical Engineering

ABSTRACT

One of the current technologies widely used to extract the earth's renewable energy is a solar module, which harnesses energy from the sun; however, its operating conditions and energy harnessing capacities vary greatly under different weather conditions. Flywheel Energy Storage Systems (FESS) present an environment-friendly solution for storing and utilizing solar energy, yet, frequent fluctuations of solar module voltage and current limit the efficiency of the FESS in photovoltaic (PV) applications. Existing literature investigates various FESS solutions for on- and off-grid PV applications; however, reported low FESS efficiency values up to 40%. Moreover, there is no commercially available FESS for off-grid or residential PV systems.

In this paper, a novel bi-directional converter is proposed to regulate the power output of the PV system to the FESS while maintaining the harnessed solar energy. A typical bi-directional converter has a fixed duty cycle that is determined based on a constant input voltage source; which is not the case with the voltage of a solar module. Hence, the proposed bi-directional converter imposes a varying duty cycle that changes based on the solar module voltage and current operating point. A fully integrated FESS, with a PV system, is modeled to simulate the overall energy harvesting capabilities. The solar module is modeled using the one-diode solar cell model technique to predict the overall system efficiency and determine the most efficient time of day for switching between the FESS's charging (morning time) and discharging mode (night time). To validate the developed solar module model experimentally, four 250-Watt Ankara Solar PV modules

are installed and field-tested. The solar insolation (solar power per square meter), wind speed, cell temperature, solar module power output, and FESS power output are logged during the system's operation. The theoretical model predicts that the total energy output for a five-day test is 27.3 kWh, while the experimental analysis shows that the solar modules produce 24.2 kWh (12% percentage difference). The average efficiency of the solar module model is determined to be 15.2%, which matches the solar module manufacturer's efficiency value of 15.4%. The theoretical power curve follows the experimental one throughout the day, which assures that the model can accurately predict the daily energy output of the solar module. The solar module simulation serves as a repeatable replication of the actual solar module source, which enables convenient, low-cost estimation of the solar module system under different environmental conditions.

The proposed bi-directional converter is modeled and integrated in the developed FESS model to determine the modified FESS power output, efficiency, and flywheel rotational speed. The FESS model is constructed based on parameters from the actual FESS being built in College Station. The daily solar energy model input is 6.75 kWh while the daily energy stored in the FESS model is 5.39 kWh, giving the proposed FESS model efficiency of 79.8%. This efficiency value is higher than both the efficiency of available lead-acid batteries (60%) and FESS (40%) in off-grid PV systems. The maximum rotational speed of the flywheel model is 300 krpm which matches the maximum rotational speed reported in the manufacturer's datasheet. After the completion of the FESS experimental setup, the integrated solar module-FESS model will be validated further against the overall experimental power output and efficiency.

DEDICATION

…to my brilliant father, Mr. Tarek Hussein; my hard-working mother, Mrs. Sahar Elatwy; my beautiful sister, Mrs. Yasmin Hussein; and my amazing brother, Mr. Marwan Hussein, for their endless love and support.

ACKNOWLEDGEMENTS

CONTRIBUTORS AND FUNDING SOURCES

Contributors

This work is supervised by a thesis committee consisting of Dr. Reza Tafreshi and Dr. Alan Palazzolo of the Department of Mechanical Engineering and Dr. Mohammad Naraghi of the Department of Aerospace Engineering.

Funding Sources

NOMENCLATURE

Solar Module Modeling

R_S	Series resistance in solar model cell circuit (Ω)
R_P	Parallel resistance in solar model cell circuit (Ω)
G	Solar insolation incident on solar module (W/m^2)
G_{ref}	Solar insolation at STC (W/m^2)
T_c	Solar module cell temperature (K)
T_{ref}	Cell Temperature at STC (K)
I	Current output of solar module cell circuit (A)
V	Voltage output of solar module cell circuit (V)
I_{ph}	Photo-generated current (A)
I_d	Diode current (A)
I_p	Leak current in the parallel resistor (A)
I_0	Reverse saturation current in the diode (A)
a	Modified ideality factor
V_T	Thermal voltage (V)
k	Boltzmann's constant (J/K)
q	Electron charge constant (C)
μ_{SC}	Temperature coefficient of short circuit current (A/K)
$I_{sc,ref}$	Short circuit current at STC (A)

$V_{mp,ref}$	Maximum point voltage at STC (V)
$I_{mp,ref}$	Maximum point current at STC (A)
$P_{mp,ref}$	Maximum point power at STC (W)
$V_{oc,ref}$	Open-circuit voltage at STC (V)
I_{array}	Current output of solar array (A)
V_{array}	Voltage output of solar array (V)
$V_{T,array}$	Thermal voltage of solar array (V)
$R_{p,array}$	Equivalent parallel resistance of solar array (Ω)
N_s	Number of solar cells in a module in series per string
N_p	Number of solar cell strings in a module in parallel
η_{ref}	Solar module efficiency at STC (%)

Flywheel Energy Storage System Modeling

E	Kinetic stored energy in flywheel (J)
I	Inertia of the flywheel (kg-m^2)
ω	Rotational speed of the flywheel (rad/s)
E_{max}	Maximum possible kinetic stored energy in the flywheel (J)
ω_{max}	Maximum possible rotational speed of the flywheel (rad/s)
σ_{max}	Tensile strength of the flywheel material (MPa)
m	Mass of the flywheel (kg)

ρ	Density of the flywheel (kg/m^3)
r	Radius of the flywheel (m)
s	Safety margin for safe flywheel operation
v_d, v_q	BLDC direct and quadrature magnetic axis voltage (V)
i_d, i_q	BLDC direct and quadrature magnetic axis current (A)
L_d, L_q	BLDC direct and quadrature magnetic axis inductance (H)
R	Stator winding resistance (Ω)
ω_r	BLDC rotor angular velocity (rad/s)
λ	Flux amplitude induced by the PM of the BLDC rotor on its stator
T_e	BLDC electromagnetic torque (Nm)
p	Number of pole pairs
J	BLDC rotor inertia (kg m^2)
F	Viscous friction on the rotor (N/kg-m)
θ	Angular position of the rotor (rad)
T_m	Shaft mechanical torque (Nm)
K_0	Torque conversion factor from mechanical to electrical energy
T	Time from flywheel maximum speed to decaying speed (s)
P_{max}	Nominal maximum power that the flywheel can sustain (W)
η_{fw}	Efficiency of the flywheel (%)

Bi-directional Converter Modeling

v_{in}	Input voltage to the converter circuit (V)
L	Inductance of the converter circuit (H)
C	Capacitance of the converter circuit (F)
R_c	Resistance of the converter circuit (Ω)
i_L	Current across the inductor of the converter circuit (A)
i_c	Current across the capacitor of the converter circuit (A)
D	PWM Duty cycle of the MOSFET
v_o	Output voltage of the converter circuit (V)

TABLE OF CONTENTS

Page

LIST OF FIGURES

LIST OF TABLES

1. INTRODUCTION

This section provides a brief introduction to the solar module system, the energy storage system, and the flywheel energy storage system (FESS), followed by a general overview of the project and its scope.

1.1. Introduction to the solar module system

Electrical power generation using Renewable Energy Sources (RES's), i.e., solar, wind, and hydroelectric, has significantly been improved over the recent years. Among these energy sources, solar energy is the most abundant and feasible to generate [1]. Solar energy production is one of the oldest and rapid increasing sources of RES, where the first single crystal silicon solar cell was developed by Bell labs in 1950 and was designed for space missions. By 1954, Bell Labs created the first modern silicon solar cell that has about 6% efficiency, and 4 years later, the first solar-powered satellite was launched with a 0.1 W, 100 cm^2 solar panel. By 1983, the worldwide photovoltaic production exceeded 21.3 megawatts (MW), and the photovoltaic production sales exceeded \$250 million. By 2013, the cumulated worldwide solar PV installations pass 100 gigawatts (GW) [2]. In 2018, the cumulative installed solar PV capacity world-wide exceeded 500 GW, and the solar energy industry topped the annual net power generating capacity out of all the current renewable and non-renewable energy sources with 102 GW [3].

With such significant development in the solar industry, the harnessed electrical energy from solar is now fed into the grid in many countries [4]. Moreover, solar modules, characterized by their self-sustainability and environment friendliness, make their

utilization a common worldwide strategy towards lower environmental impact and lower

pollutants emissions [5]. The production of solar modules has become of great interest to

the countries where there are frequent sunny days associated with high solar insolation

(amount of solar power per square meter) levels [6].

A typical solar module system consists of a solar array, a regulator, and an energy

storage device. A solar array is a series of solar modules that are composed of a set of even

smaller solar cells (shown in Figure 1) [1]. Solar cells are of three types: monocrystalline,

polycrystalline, and thin-film, each with their own characteristics summarized in [7]. In

this project, polycrystalline solar cells are used, as they are cost-efficient and widely

available in the local market [8].

Solar modules can be connected either in series, parallel, or a combination of both,

depending on the output voltage and current requirements. Solar modules which have both

series and parallel configurations are constructed by first connecting the modules in series

to form a 'string'; multiple strings are then connected in parallel to complete the solar

array. Furthermore, the generated solar module energy cannot be stored directly in an

energy storage device and has to go through a balance of systems (BOS) to bring such

harvested energy into a useful form, because the solar module power output may vary by

the weather conditions; hence, such output has to be regulated [9-12]. The balance of

systems of the solar array consists of the power regulators, wiring, and switches [12]. The

four most prominent regulators to regulate the voltage from the PV module are Shunt

Regulators, Series Regulators, Pulse Width Modulation (PWM) Regulators, and

Maximum Power Point Tracking (MPPT) Regulators [13]. In this project, the regulator used for the solar module is a MPPT regulator.
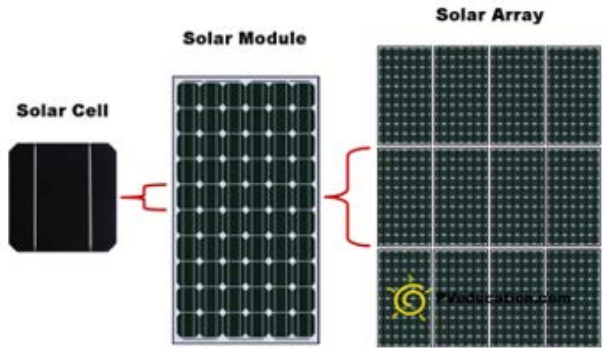
Figure 1: Solar cell, solar module, and solar array (Adapted from: [1])
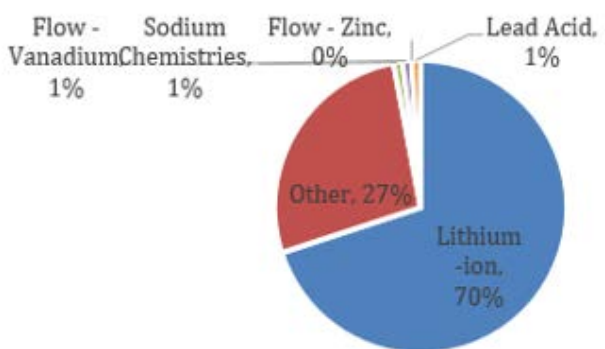
Figure 2: Battery types used in solar systems (Adapted from: [14])

1.2. Introduction to the energy storage system (ESS)

The last constituent of the solar module system is the energy storage system (ESS). The ESS is used to balance the electrical supply from the solar array and the demand from the applied load. The ESS creates this balance by converting and storing electrical energy

supplied from the solar module into another form of energy, which is then converted back to electrical energy upon demand. The use of an ESS with a solar module is necessary since the solar module's energy availability is intermittent, i.e., only available at day times. Energy storage of the solar module is cost-efficient when there is low electricity demand or low cost of electricity generation. The stored energy can then be consumed during times of high electricity demand, or at high electricity generation cost. The four forms of ESS currently available are chemical, mechanical, thermal, or magnetic [15].

According to a U.S solar energy monitor report (Figure 2) lithium-ion batteries (chemical ESS) are the most common device to store solar energy due to their ability to deliver more cycles (charge and discharge) in their lifetime than any other battery type [14]. Other solar module battery technologies such as gel, AGM, and vanadium are emerging.

1.3. Introduction to the Flywheel Energy Storage System (FESS)

A less commonly used energy storage device is a mechanical ESS, namely a Flywheel Energy Storage System (FESS), The FESS stores energy based on the rotating mass principle, where the electrical energy is converted to mechanical energy in the form of rotational kinetic energy. The FESS has existed of decades and is one of the earliest mechanical ESS [15]. The first application of the flywheel dates back to the 18th century at the beginning of the industrial revolution when they were used as an energy accumulator in steam engine boats, trains, and factories. The flywheel was then considered to be a potential ESS in the early 20th century when the rotational stresses and rotor shapes of the flywheel were studied and optimized. Finally, in the 1970s, the FESS was proposed to be

implemented in electric vehicles, in stationary backup generators, and in space [16, 17]. Despite such work, the FESS development declined as the use of an electric grid to store electric power seemed like a more cost-efficient solution [15]. However, since the recent developments in the FESS bearing material, power electronics, and electric machines, the FESS has been considered as a much more efficient and environment-friendly ESS [18-20].

The FESS is typically composed of a motor-generator (MG) coupled to a flywheel [21, 22]. The flywheel and the MG are coaxially connected, which indicates that the flywheel speed is controlled through the voltage and current input to the MG. When there is sufficient pre-determined voltage input to the MG, the MG will spin the flywheel (charging mode) [22]. Once the voltage to the motor drops below this predetermined voltage, the charged flywheel will rotate the MG's armature (discharging mode), which will turn the MG to produce AC or DC voltage (depending on the MG) [22]. This voltage can then power a typical load such as an electrical device; hence, this process may create a continuous non-interruptible power flow.

The FESS main purpose is to store energy during times when the energy from the solar module is in excess, and provide energy at urgent times to the load when the energy is in shortage. The renewable energy sources often take the form of photovoltaic cells connected to a lead-acid or lithium-ion batteries. The typical lifetime of such batteries used for the solar module energy storage application is about two years, with an efficiency of 60% or less. Moreover, these batteries are associated with environmental problems, especially in countries where there is insignificant to nonexistent recycling infrastructure.

5

On the other hand, FESS provides highly efficient, long-life energy storage solutions to the solar module system, at no environmental cost [23].

1.4. Introduction to the project scope

This project presents designing, modeling, and simulating a solar module system powering a FESS unit. The solar-module-FESS system is designed to provide electrical energy to an off-grid load, i.e., not connected to the electrical network. A 1-kW solar module model is used to supply power to the FESS. The solar module model is then validated by field-testing a 1-kW solar module system with a BOS installed in the roof of Texas A&M University at Qatar (TAMUQ). The role of the BOS (mainly battery and MPPT) is to mimic the model operation procedure, which is to maintain the solar module system at its maximum wattage output. This was completed by maintaining the battery of the BOS at a minimum state of charge; hence, the load on the solar module is kept at the maximum with the help of the MPPT. This is further explained in the Methodology section 4.2.3. The FESS was modeled as a permanent magnet MG, namely a Brushless DC (BLDC) motor coaxially connected with a composite flywheel. The flywheel is spun at very high speeds in a vacuum containment spin-pit to maximum efficiency and minimize friction losses. The solar-module-FESS design, modeling, and simulation were completed on a MATLAB/SIMULINK platform. The actual FESS contraption is being designed, built, and tested by colleagues in College Station.

2. MOTIVATION AND SCOPE

This section presents the reasons behind creating the solar-module-FESS system, and the environmental and economic benefits such a system will bring to real-life applications.

2.1. Solar module system

As discussed in the previous section, the use of solar technology as a replacement for fossil fuels has brought both an economic and an environmental benefit. Moreover, the solar module used in this project is designed to power an off-grid load with a load profile that represents that of a typical household (see section 8.3 for more details). Hence, to quantify such economic and environmental benefit with relevance to this project, a cost-benefit analysis of a substitution of a fossil-fuel-powered water heating system (WHS) to a solar WHS (SWHS) for a residential consumer was analyzed [24]. The results suggest that a SWHS installation saved $550 of electrical power (from the government) and natural gas cost per annum per household. Moreover, the SWHS saved 8329kWh of energy per annum per household, which consequently reduced 2206.9 kg CO_2, 2.08 kg SO_2 and 3.75 kg NO_x per annum per household. Hence, such implementations, when produced on a large-scale can motivate companies and governments to use more solar-powered residential applications such as the solar-module-FESS system.

2.2. Flywheel Energy Storage System (FESS)

From the FESS standpoint, this project will compare the power output and efficiency of a high-performance FESS as the primary storage component in the system as opposed to using the standard battery. Case studies [21, 25] show that the use of an FESS is

expected to have more efficient energy storage, i.e., has higher charge and discharge capabilities during its lifetime, yields a lower power loss upon storage cycles, has a longer shelf life, and is more environment-friendly compared to batteries [26]. Moreover, the solar-module-FESS combined system creates an uninterruptable power source to a suitable load that would have a longer lifetime than the traditional solar module-battery system. The current FESS technologies lose energy quickly and have a short self-discharge duration (typically 10 minutes) due to the flywheel low rotation speed and bulky material. As a result, they are less commonly used than the battery [21, 25]. Hence, to maximize FESS efficiency and reduce the associated economic constraints, optimal FESS architecture and control strategies need to be developed.

The FESS component used for energy storage provides advantages over the battery storage used in the traditional off-grid solar array systems and other various forms of energy storage systems used in the industry, as shown in Table 1. It is evident from Table 1 that the FESS technology has a longer shelf life, a higher power, and energy storage density, and has a lower environmental impact than other forms of battery storage [27].

Table 1: Performance comparison between various forms of energy storage used in industry (Adapted from: [27])

Parameter	FESS	Batteries	Gas Turbine
Efficiency (%)	~90	~70	~50
Energy storage	High	Middle	>30MW
Modularity	Yes	Yes	No
Cycle life	Unlimited	Several hundred	Several thousand
Charge and discharge time	Minute	Hour	Hour
Environmental impact	Low	Large	Large
Safety	Low	Moderate	Moderate

2.3. Solar-module-FESS system

In the field of research, there has been a continuous development towards the PV systems and the Flywheel Energy Storage Systems. The contribution of this project to this field of research is the expected increase in shelf life, efficiency, environment-friendliness, and energy storage of the combined solar-module-FESS system over the traditional solar-module-battery storage systems. This novel combination between the solar module system and the novel Nano carbon fiber high-speed FESS could prove to be a better substitute than the traditional solar-module-battery system used in off-grid operations.

The simulated solar-module-FESS systems available in the literature provide methods to model the power input, power output, and overall efficiency of the PV system and the FESS individually, with limited coupling between the solar module and FESS [23]. These existing methods do not consider the physical connection between the BLDC drive and PV system electronics. This paper provides a detailed minute-by-minute analysis of the solar- module-FESS system along with full integration between the two sub-systems.

The FESS allows for easy physical installation at the required site without any need for new transmission facilities with the solar module system. This is due to the fact the FESS is being designed and built as one compact system which includes all the interface electronics such as the microcontroller and power converters. Hence, the customer would only need to connect the output terminals of the solar module system to the FESS, and the solar-module-FESS system should run automatically. Moreover, the FESS application will enable voltage and waveform control and monitoring of the solar-module-FESS

system, which will, in turn, enhance the quality and reliability of the overall combined system power supply [23].

The solar-module-FESS system will benefit the energy sector by providing energy to applications that require continuous operation. The solar-module-FESS system could be used as a battery substitute for longer life in applications such as downhole measurement while drilling, downhole tractor operations, uninterruptible power supplies in computer data centers, or improving buildings and infrastructure and local industrial power plant energy efficiency and reliability.

The solar module theoretical modeling and experimental testing will enrich the industry and research with a solar module power output that pertains to the MENA region, and especially to the State of Qatar. The solar module field-testing setup can be used to validate any solar module model by simply connecting the same size solar modules of the model to the monitoring station in the lab. Moreover, the solar module theoretical model provides a zero-cost prediction to the daily module power output which can be used in optimization of the FESS parameters, such as maximum energy charge and discharge capabilities of the flywheel, the maximum rotation speed of the flywheel, and the overall power input and output of the FESS. The theoretical model was programmed on an open-source, widely available platform (MATLAB/SIMULINK), which can be easily integrated and used. The experimental results obtained from this project will provide the renewable energy research field with experimental data on typical solar array power output located in the Middle East.

2.4. Overall project scope

The overall project block-diagram and schematic is given in Figure 3. Each schematic is detailed individually in the following sections. The solar-module-FESS system includes the proposed BLDC bi-directional converter model which is an interface between the solar module system and the FESS. The bi-directional converter model allows for the varying voltage supplied by the solar module system to be efficiently received by the FESS and converted accordingly to kinetic energy stored in the flywheel. Once the energy output from the solar module is not sufficient for the connected load, i.e., during night time, the bi-directional converter model would direct the stored power from the FESS to the connected load. Without such interface between the two independent systems, the FESS model was not able to individually adapt to such rapid voltage variations, and the model would not converge to the desired FESS output, as shown in section 8.2. Hence, the BLDC bi-directional converter model is built with a dynamic duty cycle, i.e., it can adapt to any combination of voltage and current output of the solar module, as long as these values are within the considerable range of the power size of the solar module.
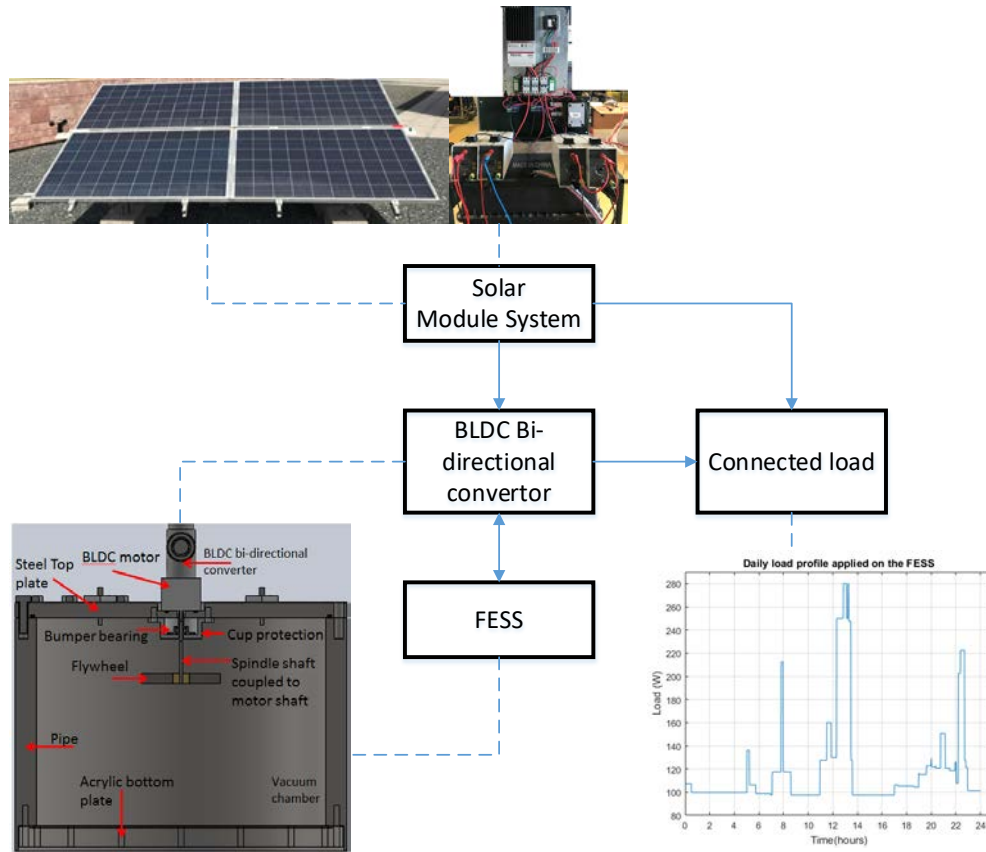
Figure 3: Overall project block diagram and individual schematics

The solar module system model, the FESS model, and the BLDC bi-directional converter model are collectively incorporated into one representative model, namely the solar-module-FESS system. Similar to the individual models, the combined solar-module-FESS system was modeled and simulated. There are two primary advantages of modeling the solar-module-FESS system. First, the solar module simulation serves as a repeatable replication of the actual solar module source, which enables convenient, low-cost estimation of the solar-module-FESS system under different environmental conditions. It will also allow for exploring new power storage applications. Second, modeling the solar

module would indicate how far off the actual solar module power output and efficiency are from the simulated results. The simulation program could then be used to initially predict the power output of the solar-module-FESS system before purchasing any solar-module-FESS equipment.

3. OBJECTIVES AND TASKS

The overall objective of this project is to design, model, simulate, and verify a solar module system and an FESS unit, and create a bi-directional converter model between the two individual subsystems. The main challenge in this objective is to create a bi-directional converter model that is able to handle the solar module system voltage rapid variations of output voltage and current. The overall objective of the project is broken down into sub-objectives presented in sections 3.1 – 3.3. The criteria chosen to evaluate each sub-objective is satisfied when each respective model (solar, FESS, or the combination of the two) is able to produce a representative output to its real-life counterpart. Each number assigned in the list of objectives is associated with the same number in its respective subsequent list of tasks. The system parameters mentioned in these sections are further explained in the following sections.

3.1. Solar module system objectives and tasks

The objectives and their respective tasks needed to complete the solar module system model and field-test are presented as follows

3.1.1. Objectives fulfilled to model the solar module system

(1) Determined the existing theoretical methods to model the solar model system based on a minute-by-minute basis, and the most effective platform that the model should be constructed on.

(2) Constructed the solar module system model based on the chosen method in (1).

(3) Verified the solar module model that it can accurately predict the actual power output throughout the day.

3.1.2. Tasks carried out to model the solar module system

(1) Conducted a literature review of the most common methods that are used to model the solar module system, and selected the model that is compatible with the FESS operation.

(2) Created a solar module model with the same parameters as the field-testing solar model system. The model takes as input minute-by-minute solar insolation and cell temperature combination and outputs the maximum voltage and current operating point of the solar module system.

(3) Performed data analysis on the model output and carried out a statistical comparison between the theoretical and experimental (presented in section 3.1.3) power output.

3.1.3. Objectives fulfilled to field-test the solar module system

(1) Determined and quantified solar module parameters, i.e., solar module system power size, open-circuit voltage, short-circuit current, solar cell type, number of modules required, and module connection arrangement (number of parallel strings, and number of series-connected modules per string).

(2) Determined and quantified BOS parameters, i.e., Battery bank size and watt-hour rating, MPPT ampere rating, and open-circuit voltage, load controller ampere rating required to protect FESS, fuse switches current rating required for over-current protection, mounting system, and wiring length and type.

(3) Determined and quantified sensory circuit specifications used to measure and record the solar insolation, cell temperature, and the solar module system voltage and current output.

(4) Obtained solar module system, BOS, and sensory circuit based on objectives (1) – (3).

3.1.4. Tasks carried out to field-test the solar module system

(1) Conducted a survey on the actual FESS to determine its voltage and power requirements in order to size the solar module system.

(2) Conducted literature review on BOS sizing based on solar module parameters mentioned in Objective (1) and consulted field engineers working in one of the local solar solutions company.

(3) Conducted literature review on the existing methods to record the output mentioned in Objective (3) and performed the required calculation to determine the specifications of the sensor.

(4) Contacted multiple local vendors and selected the vendor that is willing to provide the required solar module system and BOS with a reasonable price. The required sensory circuit equipment was purchased from online vendors based on the required sensor specifications.

3.2. Flywheel Energy Storage System objectives and tasks

The objectives and their respective tasks needed to complete the FESS model are presented as follows

3.2.1. Objectives fulfilled to model FESS

(1) Obtain the FESS model parameters, i.e., supply voltage, no-load speed, speed/torque slope, motor constant, velocity constant, damping factor, torque constant, efficiency, and rotor inertia.

(2) Constructed an initial FESS model that represents the FESS merely as a second-order mechanical system consisting of the BLDC, shaft, and inertia disk. At this stage, the charge and discharge operation of the FESS is not yet implemented in the model.

(3) Created a load profile that is suitable for the FESS power size.

(4) Incorporated FESS charge and discharge schemes into the FESS model. The source of the FESS discharge is the load profile applied in (3).

(5) Verified the charge and discharge operation of the FESS with the applied load.

3.2.2. Tasks carried out to model FESS

(1) Interview lab technician in College Station assigned on building the FESS.

(2) Conducted literature review on the theoretical equations that govern the operation of the BLDC, shaft, and inertia disk, and translated these equations into model blocks.

(3) Conducted a literature review to find typical FESS load applications that match the power size of the modeled FESS, and created a load profile accordingly. The load profile is constructed on a minute-by-minute basis, i.e., the load changes every minute of the FESS operation.

(4) Conducted literature review on theoretical equations that governs the FESS charge and discharge operations. The equations were then coded into the FESS model created in Objective (2).

(5) The FESS was verified by supplying the FESS with a constant voltage source and comparing the FESS output to typical FESS output in literature.

3.3. BLDC bi-directional converter model objectives and tasks

The objectives and their respective tasks needed to complete the proposed BLDC bi-directional converter model are presented as follows

3.3.1. Objectives fulfilled to model the BLDC bi-directional converter

(1) Created a combined non-converging solar-module-FESS model into a model.

(2) Constructed a varying BLDC duty cycle plot which causes the varying voltage and current output by the solar module to produce a converging FESS power output.

(3) Created a representative converging solar-module-FESS system

3.3.2. Tasks carried out to model the BLDC bi-directional converter

(1) Created a direct connection between the solar module system model and FESS model blocks.

(2) Proposed a model which converts every voltage and current output combination from the solar module system into a different combination that converges the FESS model. The conversion factor for every combination was stored and is termed the duty cycle.

(3) Implemented the varying duty cycle conversion into the BLDC of the FESS, which is the recipient of the solar module system voltage and current output.

4. SOLAR MODULE MODELING

The solar panel module system is modeled based on the literature review and the methodology presented in the following sections. The model was established by first developing the mathematical formulation of one solar cell circuit, then scaling that circuit to represent the entire solar module system.

4.1. Theory

Solar module modeling pertains to characterize the solar module power output as a mathematical formulation, relating the voltage to the current output of the solar module, i.e., obtaining the I(V) curve. To obtain the solar module mathematical formulation, one may construct a solar cell equivalent circuit [28]. There are various solar cell equivalent circuits in literature, each characterized by its own set of parameters; however, the most prominent one is the one-diode circuit shown in Figure 4 [28]. The full list of parameters is explained later in this section.

The one-diode solar cell circuit is mostly used for solar module modeling in power systems, as it is computationally inexpensive, due to a lower number of unknowns and iterations used in the calculation [29, 30]. The one-diode solar circuit is the preferable solar model type for the FESS model, as the FESS model would require the solar model to be performed minute-by-minute over the day. Other circuits such as the two-diode circuits are mainly used for high-accuracy prediction of solar module output to study the module's cell characteristics at critical points [30]. To quantify, at 50°C (the average operating temperature range of the solar module in this project) the solar module model

based on the one-diode circuit had a 0.9% and 0.5% error in estimating the maximum

power of a ShellST40 and a Shell SP_70 solar modules respectively; while the solar

module model based on the two-diode circuit had 0.7% and 0.3% error [31, 32]. However,

the computation time for the model based on the one-diode circuit was 2535 milliseconds,

while the model based on the two-diode one was 3320 milliseconds. Hence, such a small

increase in model prediction error (0.2% error increase between the one- and two- diode

circuits), lower number of unknowns, and faster computation time preferred the use of a

one-diode over a two-diode circuit in this project [32-34].
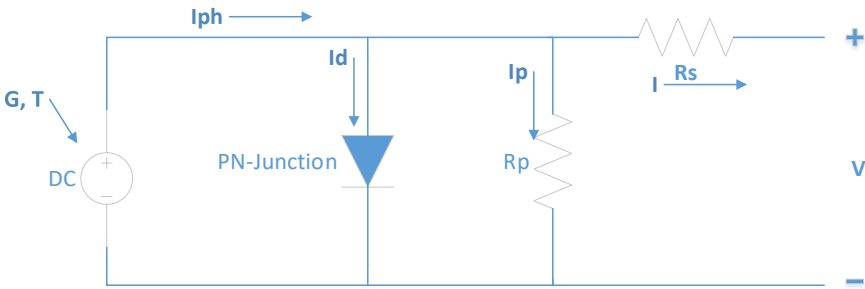
Figure 4: One-diode equivalent circuit with series and parallel circuits (Adapted from: [35])

The parameters of the solar module model based on the one-diode circuit are either

provided by the manufacturer or are unknown (mainly as resistances to represent losses)

and have to be calculated or assumed [36, 37]. Those provided by the manufacturers

usually do not provide sufficient information on their correlation to the weather

conditions, such as solar cell temperature and solar insolation; hence, more assumptions

regarding the cell behavior concerning its physical nature are required to create the solar

module model [36]. Some literature assumed these parameters constant, while others consider their variations as negligible. For instance, Benmessaoud et. Al. (2010) [38], Bouzid et al. (2005) [39], and Walker and Geoff (2001) [40] included the series resistance, but not the parallel resistance. Many others ignored both resistances by setting the series resistance as very low and the parallel resistance very high. On the other hand, Bellia et al. (2014) [41] and Chouder et al. (2012) [42] took into account both resistances.

In the one-diode circuit shown in Figure 4, R_S and R_P represents the series and parallel (shunt) resistances, respectively [43]. The PN-junction represents the bypass diode that is installed in the actual solar cells to minimize the voltage loss that may occur during complete or partial shading of the solar module (the path between the sun and the solar module is blocked by a cloud or by an object). The series resistance represents losses in cell solder, bonds, interconnection, and junction box [44]. The shunt resistor represents the current leakage through the high conductivity shunts across the p-n junction (diode) of the solar module [44]. G and T_c represents solar insolation and cell temperature, respectively; I_{PH} is the photo-generated DC current source which depends on both G and T_c [43]. I and V are the output of the solar cell needed for the $I(V)$ curve.

4.1.1. Solar cell circuit

By applying Kirchhoff's current law of the circuit shown in Figure 4:

$$I = I_{ph} - I_d - I_p; \tag{1}$$

where I_d is the diode current, and I_P is the leak current in the parallel resistor. The governing equation of the circuit would then become:

21

$$I = I_{ph} - I_0 \left[\exp\left(\frac{V + I R_s}{a}\right) - 1 \right] - \frac{V + R_s I}{R_P} \tag{2}$$

where I_0 is the reverse saturation current, and a is the modified ideality factor given as:

$$a = A\, V_T; \quad V_T = \frac{k\, T_c}{q} \tag{3}$$

where A is the PV ideality constant = 1.3 for Si-poly cells (the solar cell type used in this project), V_T is the thermal voltage, k is the Boltzmann's constant, and q is the electron charge. Equation (2) is the most commonly-used equation that governs the voltage and current output of the solar cell [44]. To solve for I in Equation (2) for a given V, one has to compute first the constituent parameters a, I_0, I_{ph}, R_s, and R_p, for every solar insolation and cell temperature combination.

4.1.2. Determination of the circuit model parameters (I_{ph}, I_0, and R_P)

Authors in [41] provided a detailed method to solve for the four parameters, a, I_0, I_{ph}, R_s, and R_p, in Equation (2). The thermal voltage, a, can be computed from equation (3). The photocurrent I_{ph} depends on the input cell temperature and solar insolation:

$$I_{ph} = \frac{G}{G_{ref}} \left(I_{sc,ref} + \mu_{sc}\, \Delta T \right) \tag{4}$$

where subscript '*ref*' refers to a reference at Standard Test Conditions (STC), usually provided by the manufacturer. G: Solar insolation (W/m^2); G_{ref}: Insolation at STC = 1000 (W/m^2); $\Delta T = T_c - T_{ref}$ (Kelvin); T_{ref} = Cell Temperature at STC = 298 K; μ_{SC}: Temperature coefficient of short circuit current (Amps/K); $I_{sc,ref}$: Short circuit current at STC. μ_{SC} and $I_{sc,ref}$ are constants provided by the manufacturer shown in Table 2.

The reverse saturation current, I_0, is given by:

$$I_0 = I_{sc,ref} \exp\left(\frac{-V_{oc,ref}}{a}\right)\left(\frac{T_c}{T_{ref}}\right)^3 \exp\left[\left(\frac{\left(\frac{q\,\epsilon_G}{A\,k}\right)}{T_{ref}} - \frac{\left(\frac{q\,\epsilon_G}{A\,k}\right)}{T_{cell}}\right)\right] \tag{5}$$

ϵ_G: Material band-gap energy $= 1.12$ eV for Silicon.

R_P to R_S can be related so that the computed maximum power P_{mp} is equal to the experimental one $P_{mp,ref}$ [41]:

$$R_P = \frac{V_{mp,ref} + I_{mp,ref}R_S}{I_{sc,ref} - I_{sc,ref}\left\{\exp\left[\frac{V_{mp,ref} + R_S\,I_{mp,ref} - V_{oc,ref}}{a}\right]\right\} + I_{sc,ref}\left\{\exp\left(-\frac{V_{oc,ref}}{a}\right)\right\} - \left(\frac{P_{mp,ref}}{V_{mp,ref}}\right)} \tag{6}$$

The subscript '*mp,ref*' refers to the respective parameter at the maximum power point, which is usually provided by the manufacturer. $V_{oc,ref}$ is the open-circuit voltage at reference, which is also provided by the manufacturer. Equation (6) can be solved using the Newton-Raphson method. Note that for a different instance of time, the thermal voltage, a, will change, which will change the (R_S, R_P) combination accordingly. Hence, Equations (4), (5), and (6) must be solved simultaneously.

4.2. Methodology

4.2.1. Model implementation for obtaining I(V) curves

An array of four 250-W solar modules are used in this project. The module's specifications and parameters provided by the manufacturer are presented in Table 2. As seen in Table 2, each solar module has 6 solar cells in series in each branch and a total of 10 parallel-connected branches (= 60 solar cells in total in each module). Moreover, in the array of four modules, there are two series-connected modules per string, and there are 2

parallel strings. Hence, Equations (2) to (6) are scaled according to Equation (7) to obtain

a representative I(V) characteristic of the solar array.

$$I_{array} = 2N_p\ I; \quad V_{array} = 2N_s\ V; \quad V_{T\ array} = 2N_s\ V_T;$$

$$R_{s,array} = \frac{N_s}{N_p}\ R_s; \quad R_{p,array} = \frac{N_s}{N_P}\ R_p \qquad (7)$$

Equations (2) to (7) are programmed and implemented to obtain the I(V) curves with

the aid of the built-in SIMSCAPE Power Systems Specialized Technology Renewable

Energy block library [45]. The pseudocode flowchart that the solar module software is

programmed to follow is shown in Figure 5. Figures 6 to 8 show the block and sub-block

diagrams implemented in SIMULINK to obtain the I(V) curves.

Table 2: Ankara Solar AS-6P solar module (250 W) characteristics

Parameters	Description	Value
$P_{MP,ref}$ (W)	Power output at MPP	250
$I_{MP,ref}$ (A)	Current output at MPP	8.26
$V_{MP,ref}$ (V)	Voltage output at MPP	30.3
$I_{SC,ref}$ (A)	Short circuit current	8.75
$V_{OC,ref}$ (V)	Open circuit voltage	38.0
η_{ref} (%)	Solar module efficiency	15.37
Solar cell type	Polycrystalline	-
Ns	Number of series-connected cells in each branch	6
Np	Number of parallel-connected branches	10
Module dimension	-	1640x992x40 mm
μ_{SC} (A/K)	Temperature coefficient at short circuit	0.0049
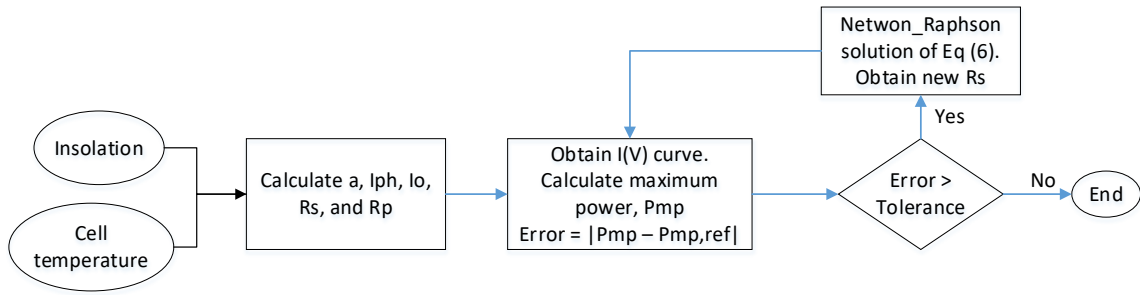
Figure 5: Iteration flowchart for obtaining the I(V) curve
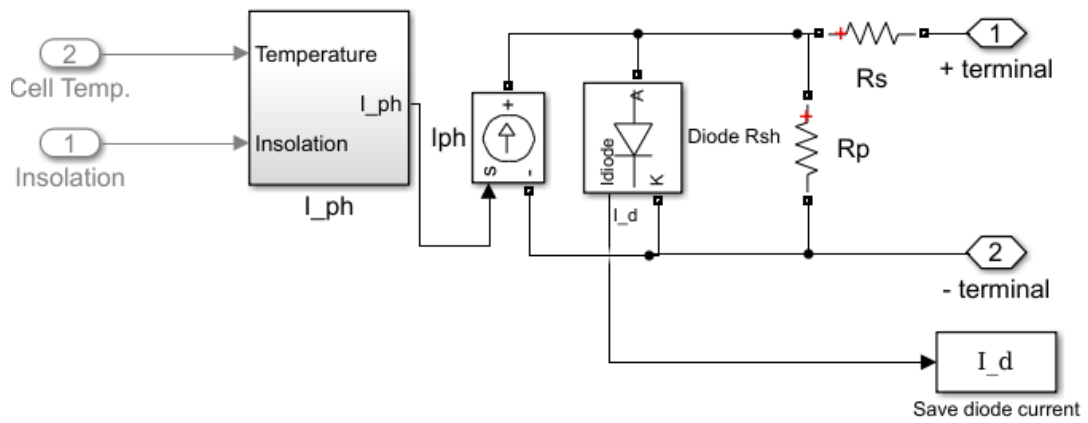
Figure 6: Model to obtain I(V) curve from Equation (2)

25
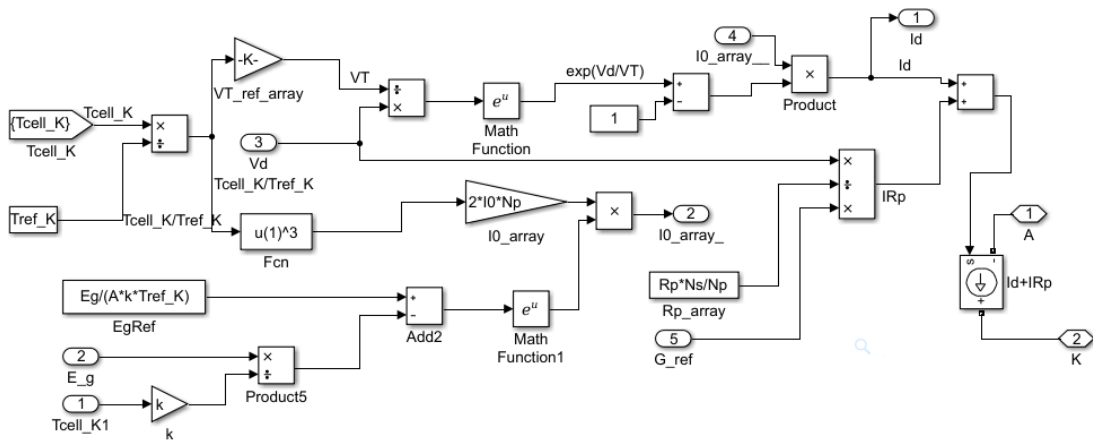
Figure 7: I_d sub-block used in Equation (5)

SIMULINK of Equation (4)
Iph = G/Gref * Np(Isc_ref + mu_sc(delta T)
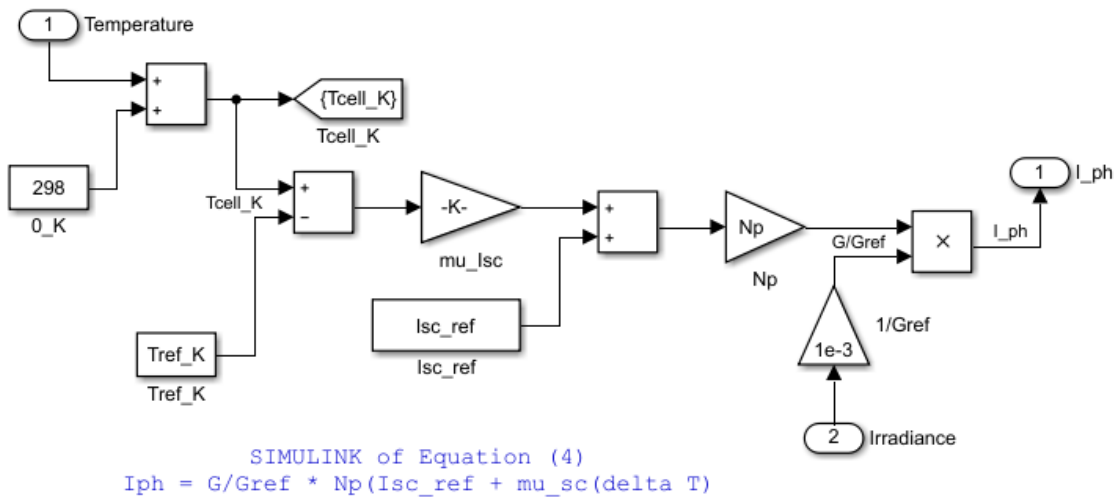
Figure 8: I_{PH} sub-block used in Equation (4)

As Figure 6 shows, the input to the solar module model is a solar insolation value and a cell temperature operating point. This combination is fed to the model, and the output is the corresponding I(V) curve. The solar insolation and cell temperature data are measured using the weather sensors detailed in section 5.1.

26

4.2.2. Model implementation for obtaining MPP current and voltage

To simulate the solar module system operation for five days, on a minute-by-minute

basis, the simulation was performed 7200 times (= 5 days * 24 hours/day * 60 minutes*

hour), i.e., 7200 input combinations of solar insolation and cell temperature, and resulting

in 7200 I(V) curves. Real-life solar module systems are designed to operate at the

maximum power point (MPP) with the help of a maximum power point tracker MPPT. To

mimic such consideration in the model, the MPP of each of those of 7200 I(V) curves are

selected for each corresponding solar insolation and cell temperature combination by

performing a sweep of each individual I(V) curve and calculating the respective MPP of

each curve. Figure 9 shows the model implemented to sweep each individual I(V) curve

to produce the maximum current and voltage combination (MPP). Hence, the overall

output of the solar module model is a vector of length 7200 showing the maximum power

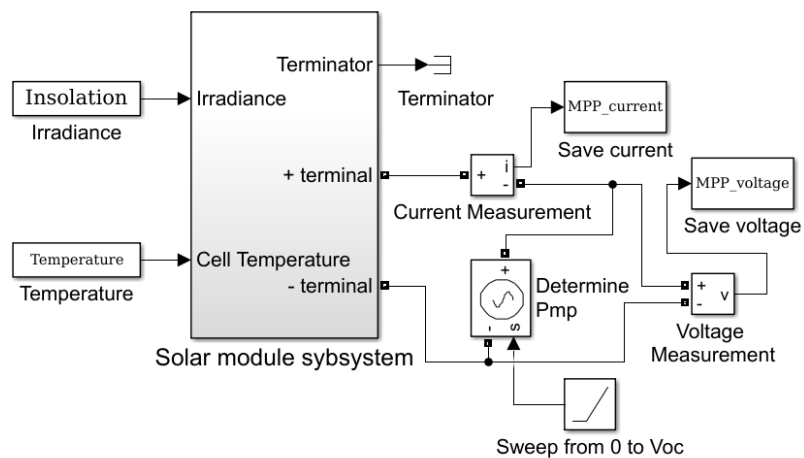point voltage and current output over the five-day period.

Figure 9: I(V) curve sweep to produce the MPP

5. SOLAR MODULE FIELD-TESTING

Solar module field-testing was performed to experimentally verify the power output of the solar module model presented in the previous section

5.1. Experimental setup

Field-testing the solar module is beneficial in determining the experimental MPP power and the efficiency of the solar modules. Field-testing initially helps to predict the most efficient switching instance between charging and discharging the flywheel, before using the solar module simulation to predict such a task more accurately. Field-testing the solar module system can determine the charge efficiency of the batteries that can be later compared to the effectiveness of the FESS. The field-testing results have been acquired through a LabVIEW platform. The block diagram of the solar module system is shown in Figure 10.

An array of four 250-Watt solar modules are installed on the roof of TAMUQ. The solar module parameters are given in Table 2. The solar modules are connected to a MPPT that is located in a lab downstairs through a conduit that goes through the ceiling. The MPPT tracks and outputs the voltage and current MPP. A battery pack that consists of two series-connected 12-V 300-Ah GEL batteries is then connected to the MPPT. The batteries are kept at their minimum state of charge (SOC), i.e., fully discharged, to ensure that the MPPT always outputs the highest possible current and voltage MPP. The minimum SOC is achieved by four parallel-connected 13-Ohm power resistors that are always connected

28

to the battery pack. In the real-life application of the solar-module-FESS system, the battery pack is to be replaced with the fabricated FESS system.

The sensors used to monitor this entire setup, each along with their description, are summarized in Table 3. The setup located in the lab is shown in Figure 11 (a). The setup located on the roof is shown in Figures 12(a) - 12(d). The solar insolation and wind speed sensors (Figure 12 (b), (c)) are mounted using 3D printed parts manufactured from TAMUQ's rapid manufacturing lab. Two data loggers are utilized for recording the sensors data, one associated with the sensors on the roof, and one associated with the sensors in the lab, as indicated in Table 3.

The data acquired from the sensors in the lab are logged using the National Instruments Data Acquisition (NI DAQ). The LabVIEW virtual interface (VI) that is used to acquire the signals from the NI DAQ is shown in Figure 11 (b). Using the values from the current and voltage sensors, power output and efficiency vs. time graph can then be generated (using $P = I*V$). The resulting graphs are validated against the results from the sensors on the roof (weather sensors), i.e., a sudden drop in insolation would result in a decline in the solar module power output.

Three 20-A fuse-switches and a load controller are installed to maintain safe operation of the solar module system, as shown in Figure 10. One fuse-switch was installed between the solar module and the MPPT to protect the MPPT from any current spikes that may occur from the solar module. Another fuse-switch was installed between the battery pack and the MPPT to preserve the battery pack from any short-circuit that may occur, especially during night time when the solar modules are not producing any power. The

29

last fuse-switch is installed between the battery pack and the load controller to protect the

connected power resistors from any short-circuit that may occur from the battery pack.

The load controller is connected between the battery pack and the power resistors to help

regulate the voltage output from the battery pack, as any over-voltage may cause overheat
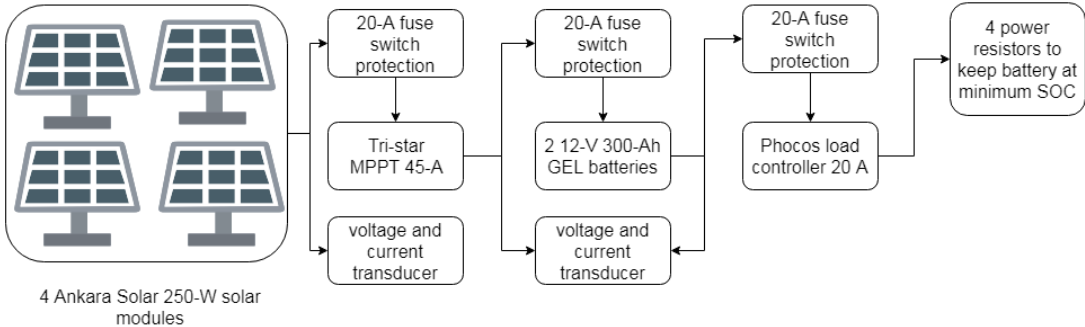
and damaging to the power resistor.

Figure 10: Schematic diagram of the solar module field-testing system

Table 3: Summary of all the equipment for field-testing the solar module system

Sensor and Parameter Measured	Figure	Specifications
Sensors and Data Acquisition located on the solar modules on the roof		
Apogee SP-110 Pyranometer sensor to measure insolation (solar power per square meter)		Calibration factor: 5 W m-2 per mV Sensitivity: 0.2 mV per W m m-2 Uncertainty: 5 % Output range: 0 to 400 mV Non-linearity: up to 2000 W m-2
TM-V-4090 Solar module cell temperature sensor with analog output		Output range: 0 to 10 V at -40 to +90C Uncertainty: 1 Kelvin Power supply: 12 to 28 VDC Sensor element: Pt1000 Class A Current: 5 mA; Load (DAQ): min 10 kOhms
Adafruit Anemometer wind speed sensor w/ analog voltage output		Output range: 0.4 V to 2 V Input range: 0.5 m/s to 50 m/s Accuracy: 1 m/s Power supply: 7 – 24 VDC
DataTaker DT80 smart data logger for roof sensors		5 independent analog input channels 10 to 30 VDC voltage supply 40 Hz max sample speed
Sensors and Data Acquisition located in the lab		
2 DC current transducers with hall effect to measure current output		Power supply: 20 – 45 VDC Input current range: 0-50 A Accuracy: 0.5 A Output signal: 4-20 mA Output load: 500 Ohms max
2 DC voltage transducers to provide an output DC signal that is proportional to the input DC voltage		Power supply: 24 VDC 10% Output signal: 0 – 10 V Accuracy: 1.0% full-scale Linearity: 10 to 100% full scale
NI-Data Acquisition NI-9263		Self-powered DAQ LabVIEW programming software 9 independent analog input channels

31
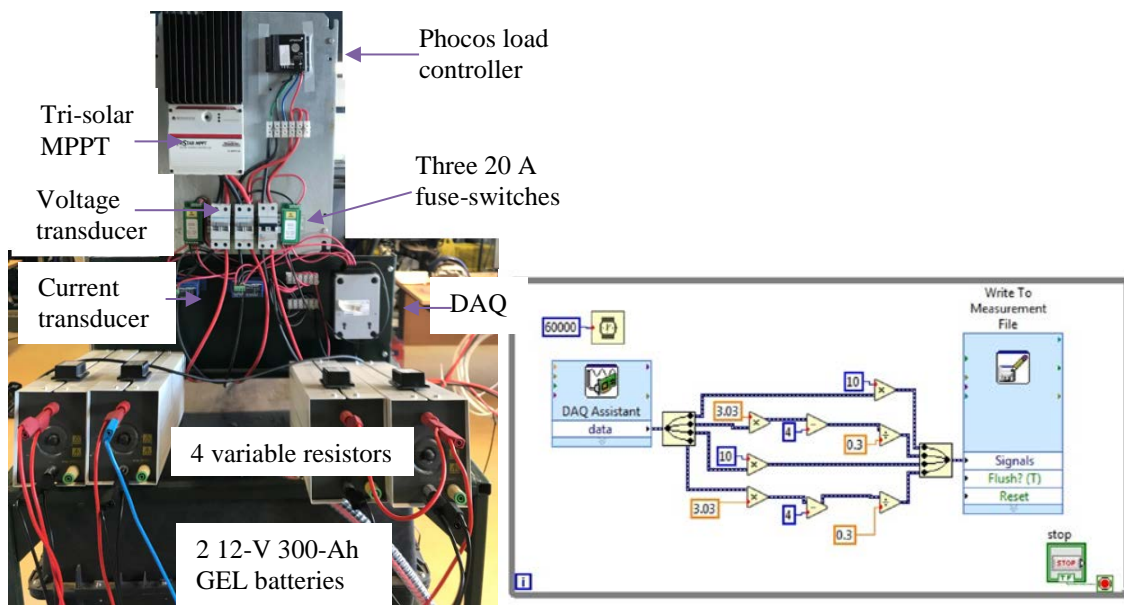
Figure 11: (a) Setup of the sensors and equipment located in the lab (b) LabVIEW VI to log data from NI-DAQ

(a)

(b)

(c)

(d)
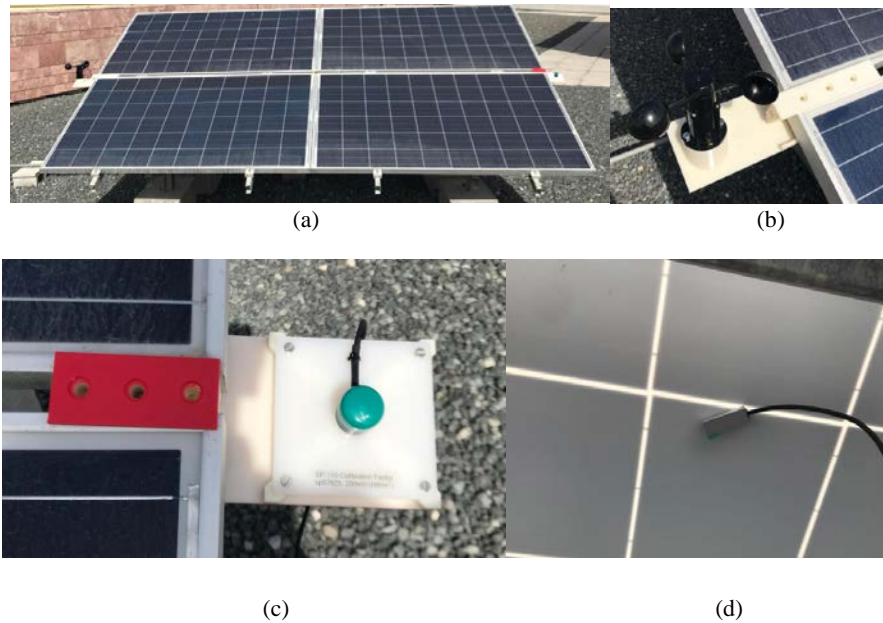
Figure 12: (a) The solar array located on the roof of TAMUQ (b) wind speed sensor with mount on the module (c) pyranometer with mount on the module (d) Cell temperature probe on the back of the module

5.2. Field-testing operating procedure

(1) Connect two parallel strings of solar modules, with two series-connected modules per string to create the solar array.

(2) Connect the array terminals to the voltage and current transducers. Connect the transducers data output to the NI-DAQ.

(3) Connect the array terminal to the MPPT input with 20-A fuse-switch protection between them.

(4) Connect the MPPT output to the 2 12-V battery pack with 20-A fuse-switch protection between them.

(5) Connect the MPPT output to the voltage and current transducers. Connect the transducers data output to the NI-DAQ.

(6) Connect the battery pack to the load controller, and then connect the load controller to the four 13-Ohm power resistors.

(7) Install the three 20-A fuse switches, as indicated in Figure 11. The fuses are kept in an off position.

(8) Install the pyranometer, wind sensor, and cell temperature sensor. Connect the sensor data output to the dataTaker DT80 DAQ.

(9) Turn on the three fuse-switches to begin the experiment. After five days (=24*5 hours) turn off the three fuse-switches to conclude the experiment. The sensor and transducer data are saved on an XLS spreadsheet.

6. FLYWHEEL ENERGY STORAGE SYSTEM MODELING

The typical FESS consists of a motor-generator (MG) electrical machine, a flywheel rotor, a bi-directional converter, thrust bearings, a rotating shaft, and a vacuum enclosure spin pit. Figure 13 shows the FESS constituents. The FESS operating theory and modeling procedure is detailed in the following sections.
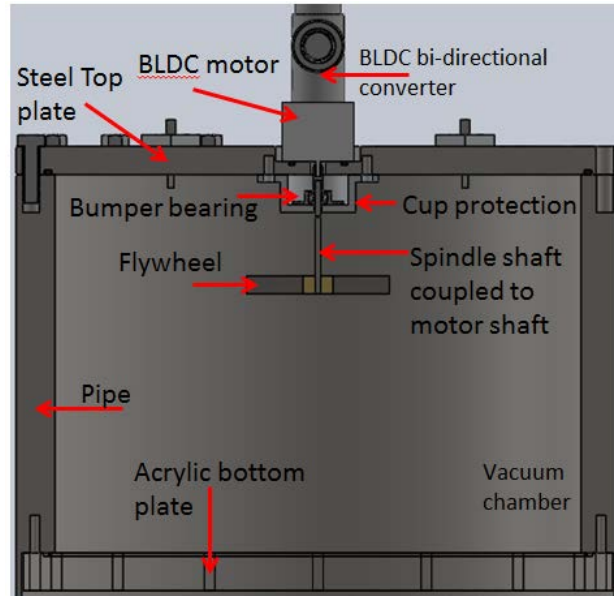
Figure 13: Schematic diagram of the FESS.

6.1. Theory

The theoretical equation governing the operation of the flywheel rotor, electrical machine, and discharge scheme are presented in the following subsections.

6.1.1. Flywheel rotor

The stored kinetic energy in the flywheel disk is governed by the flywheel rotor dimension and material. Flywheels are constructed as solid or hollow cylinders with various cross-sections, as seen in Figure 14 [46].
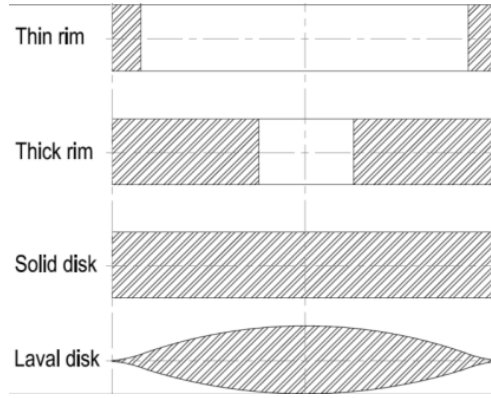
Figure 14: Typical flywheel cross-sections used for the construction of a FESS (Adapted from: [46])

The flywheel rotor used in this project is of a solid cylinder type composed of a novel carbon-fiber composite which enables the flywheel to be spun to very high speeds; hence, improving the overall FESS efficiency. The stored kinetic energy, E, is proportional to the inertia, I, and to the square of its rotational speed, ω, as shown in Equation (8) [47, 48]. To maximize the energy storage in the FESS, the flywheel is assumed to spin at the highest possible angular speed, ω_{max} [49]. The inertia of a solid-cylinder flywheel with mass m, density ρ, radius r, is expressed as $I = \frac{1}{2}mr^2$:

$$E = \frac{1}{2}I\omega^2; E_{max} = \frac{1}{2}I\omega_{max}^2 = \frac{1}{4}\pi\rho h\omega_{max}^2 r^4; \quad \omega = \sqrt{\frac{2E}{I}} \qquad (8)$$

35

The term ω_{max} is dictated by the material parameters of the flywheel. Since the flywheel material used in this project is novel, ω_{max} was estimated from Equation (9), where σ_{max} is the tensile strength of the flywheel material, s is the safety margin for safe flywheel operation. These details were obtained from the researchers developing the said novel flywheel [50]. Equation (8) indicates that the flywheel stored energy is optimized by either increasing the rotational speed or increasing the moment of inertia.

$$\omega_{max} = s \, \frac{1}{r} \sqrt{\frac{\sigma_{max}}{\rho}} \,; \qquad\qquad (9)$$

Increasing the rotational speed is preferable as it scales the energy stored by the square of the speed; however, high speeds induce higher rotational stresses as indicated by Equation (9) [51]. Therefore, the novel carbon-fiber composite is being used to construct the FESS model.

6.1.2. BLDC motor-generator (MG)

The flywheel is co-axially coupled to the MG which enables the solar module electrical energy conversion and the charge-discharge process of the FESS. The MG that is used in this project is a BLDC permanent magnet (PM) motor. The PM is the most commonly used machine for FESS application due to its higher efficiency, higher power density, and lower rotor losses than the other available electrical machines such as the induction machine (IM) and the variable reluctant machine (VRM) [46, 52].

The equations of motion that govern the operation of the PSMS are shown in Equations (9) – (12), where v_d, i_d, L_d and v_q, i_q, L_q are the BLDC q and d axis voltage, current, and inductances, respectively. R is the stator winding resistance. ω_r is the BLDC rotor angular

velocity. λ is the flux amplitude induced by the PM of the BLDC rotor on its stator. T_e is the BLDC electromagnetic torque. p is the number of pole pairs. J is the BLDC rotor inertia. F is the viscous friction losses on the rotor. θ is the angular position of the rotor. T_m is the shaft mechanical torque [51, 53]. The $\pm$ sign in Equation (12) indicates the mode of operation of the FESS (+ sign for motor mode, and – sign for generation mode):

$$\frac{d}{dt}i_d = \frac{1}{L_d}v_d - \frac{R}{L_d}i_d + \frac{L_q}{L_d}p\omega_r i_q \tag{9}$$

$$\frac{d}{dt}i_q = \frac{1}{L_q}v_q - \frac{R}{L_q}i_q - \frac{L_d}{L_q}p\omega_r i_d - \frac{\lambda p \omega_r}{L_q} \tag{10}$$

$$T_e = 1.5p\left[\lambda i_q + \left(L_d - L_q\right)i_d i_q\right] \tag{11}$$

$$\frac{d}{dt}\omega_r = \frac{1}{J}\left(T_e - F\omega_r \pm T_m\right); \qquad \frac{d}{dt}\theta = \omega_r \tag{12}$$

6.1.3. FESS discharging operation

The FESS discharge theory dictates how the BLDC outputs energy to the connected load. The load that is connected to the BLDC is discussed further in the Results and Discussion section 8.3. The angular speed during the discharge of the FESS could be stated as a piecewise-defined function as shown in Equation (13), where K_0 is the torque conversion factor from mechanical to electrical energy, and T is the time it takes the flywheel to transition from the ω_{max} speed to the decaying speed. T is determined by Equation (13), where P_{max} is the nominal maximum power that the flywheel can sustain. Plugging Equation (13) into Equation (8) and taking the derivative with respect to time produces the flywheel discharging power characteristics shown in Equation (14). The term η_{fw} represents the efficiency of the flywheel, and which determines the required power to

keep the flywheel spinning before stopping, i.e. the flywheel standby loss. Literature shows that η_{fw} ranges between 95% to 98% [49, 54].

$$\omega(t) = \begin{cases} \omega_{max} \; ; & t \geq T \\ \omega_{max} \exp\left(-\dfrac{K_0}{I} t\right) \; ; & t \geq T \end{cases}; \quad T = \dfrac{J \, \omega_{max}^2}{2 \, P_{max}} \tag{13}$$

$$P(t) = \begin{cases} P_{max} \; ; & t \geq T \\ \eta_{fw} \, \omega_{max}^2 \exp\left(-\dfrac{2K_0}{I} t\right) \; ; & t \geq T \end{cases} \tag{14}$$

6.2. Methodology

The FESS model was constructed based on the theory presented in Equations (8) to (14) with the aid of the power systems SIMSCAPE components [55]. The FESS model contained the solar module output as the DC power supply to the FESS, an inverter to convert the DC power input to 3-phase as required by the BLDC motor, the BLDC MG, and the flywheel inertia disk. The inputs to the FESS simulation were the voltage and current output from the solar model; while the output of the simulation is the flywheel power output (kW), energy output (kWh), and rotating speed (krpm). The parameters that were used to model the FESS are presented in Table 4. The parameters that were required as user-input to complete the simulation which was not included in the manufacturer's datasheet were the maximum flywheel speed (krpm), power capacity (kW), energy capacity (KWh), charge and discharge durations at maximum power and half of maximum power. The model was validated by comparing the solar module's and the FESS instantaneous power curve and the total energy outputs. The overall FESS model showing the inverter, the BLDC, and the flywheel is presented in Figure 15.

Table 4: Parameters used to model the FESS

| FESS model components	
Brushless DC motor	
Nominal supply voltage	24 V
Speed/torque slope	3753521 rpm/Nm
Motor constant	0.00211 Nm/(w$^{1/2}$)
Damping factor	1.8*10^{-6} Nm/krpm
Velocity constant	8333 rpm/V
Torque constant	0.0011 Nm/A
Maximum efficiency	86%
Maximum permanent magnet flux linkage	0.03 Wb
Rotor angle over which back EMF is constant	π/12 rad
Number of pole pairs	6
Stator d-axis inductance	0.00022 H
Stator q-axis inductance	0.00022 H
Stator zero-sequence inductance	0.00016 H
Stator resistance per phase	0.013 Ohm
Rotor inertia	7.84*10^{-8} kg m^2
No-load speed	300 krpm
Flywheel	
Material density (carbon fiber)	1938.5 kg/m^3
Flywheel mass	0.37 kg
Flywheel thickness	0.254 m
Flywheel diameter	0.096 m
Maximum rotation speed	300 krpm
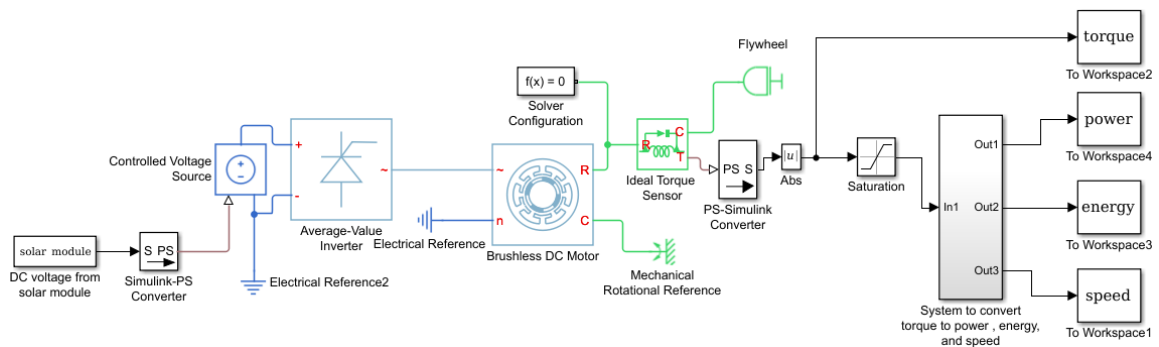
Figure 15: Implemented FESS model

7. BI-DIRECTIONAL CONVERTER MODELING

The proposed BLDC bi-directional converter model detailed in the following subsections provides an efficient interface between the solar module model and the FESS model.

7.1. Theory

As mentioned earlier, the integrated motor-generator (MG) in the FESS is the BLDC. The BLDC accelerates and decelerates the flywheel through the bi-directional converter as shown in Figure 3. The primary function of the bi-directional converter is to regulate the voltage input to the FESS and to determine the switching instances of the BLDC from motor mode to generation mode and vice-versa. The switching devices of the bi-directional converter model which determine the switching instances is selected in this project to be a combination of metal oxide semiconductor field-effect transistor (MOSFET) and insulated gate bipolar transistor (IGBT). MOSFETs and IGBTs have been widely used due to their higher switching frequencies and higher power capabilities [16]. The bi-directional converter model controls the ratio between the input voltage and the regulated output voltage; this ratio is termed the duty cycle of the MOSFET and IGBT, D [56]. The bi-directional DC-DC circuit chosen in this project is a non-inverting buck-boost converter because this converter type allows for a wide operating range for input and output voltages, which is a characteristic of the solar module system [57]. The bi-directional converter model should provide both step-up and step-down operation modes, depending on the BLDC M/G mode of operation [57]. Hence, the non-inverting buck-

boost can meet those requirements as it can operate as a buck (step-down during FESS charge mode), buck-boost (used during the instance of switch from M to G or vice-versa), or boost (step-up during FESS discharge mode) [58]. The non-inverting buck-boost circuit is shown in Figure 16.
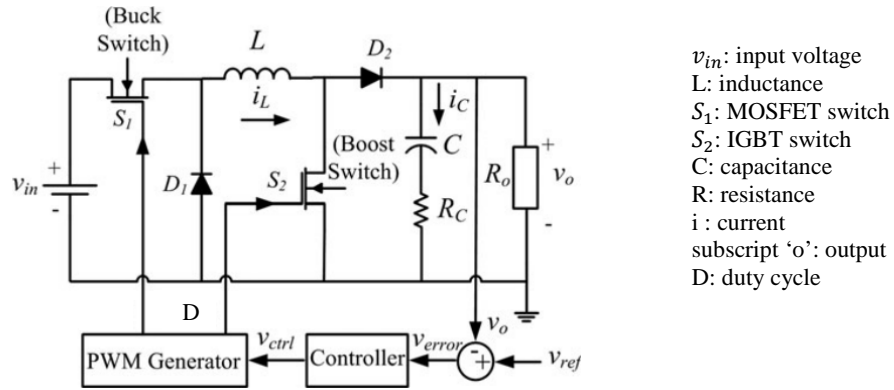
Figure 16: Non-inverting buck-boost bi-directional converter with a control system (Adapted from: [56])

The output voltage and current of the buck-boost bi-directional converter model are given in Equation (15), where, again, D is the duty cycle of the MOSFET.

$$V_{out} = \frac{D}{1-D}V_{array}; \quad I_{out} = \frac{1-D}{D}I_{array}; \quad \therefore \frac{V_{array}}{I_{array}} = \left(\frac{1-D}{D}\right)^2 R_{out} \qquad (15)$$

7.2. Methodology

In Equation (15), the subscript 'array' means the input to the BLDC bi-directional converter model, i.e., the voltage and current output of the solar module, which are known parameters. The term R_{out} is the equivalent resistance of the FESS and is determined based on iterations of (9) – (11) at the maximum speed of the flywheel, i.e., the duration

41

when the FESS has the highest equivalent resistance value. The non-inverting buck-boost converter (shown in Figure 16) was modeled with the aid of SIMSCAPE Power Electronics built-in library and is shown in Figure 17 [59]. For each of the 7200 solar insolation and cell temperature combinations, the modified load resistance of the FESS was computed, then the duty cycle D was calculated through Equation (15). A plot of the duty ratio versus modified load resistance was constructed and could be used as the BLDC bi-directional electronics interface for different FESS models. The modified voltage and current output of Figure 17 are used as the new inputs to the FESS model shown in Figure 15.
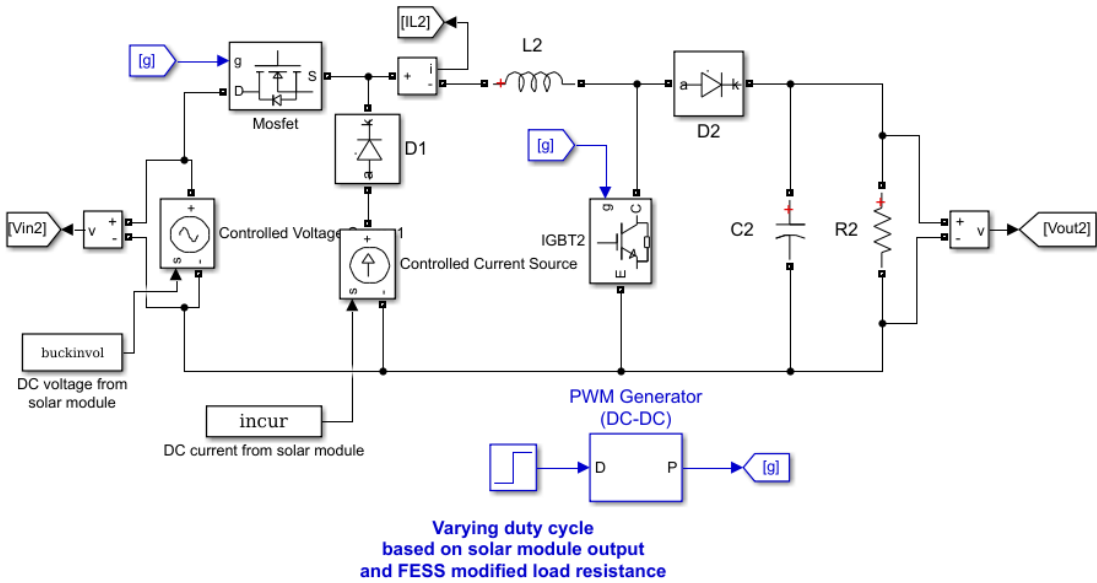

Figure 17: The non-inverting buck-boost converter model with varying duty cycle (Adapted from: [59])

8. RESULTS AND DISCUSSION

The results and analysis presented in this section are divided into three main steps: the solar module model and field-testing, the proposed BLDC model bi-directional converter model, and the results of the combined solar-module-FESS system.

8.1. Solar module model validation using field testing

The solar module model operating principles was based on the theory presented in section 4.1, and the model was constructed based on the methodology outlined in section 4.2. The solar module field-testing was performed using the methodology outlined in section 5. The solar module model voltage, current, and power output were validated against the field-testing output for a five-day period. Moreover, the insolation (solar power produced by the sun per square meter) and solar cell temperature data for this period were also recorded to justify any discrepancies in the results. The data was recorded during the fall season from 4/12/2019 at 5 AM and 4/16/2019 at 6 PM at every minute. The solar module model and field-testing results are shown in Figures 18 to 21.

Figure 18 shows that the insolation and cell temperature data which are measured by the pyranometer and cell temperature sensors described in section 5.1, respectively. The insolation and cell temperature data have a positive correlation. The insolation and the cell temperature reached a maximum value of 1150 W/m^2 and 59°C, respectively, which indicates the hot and sunny weather environment that the solar modules were located at. During noontime of the second day, the insolation and cell temperature had a drastic drop

which could be attributed to partial shading by a cloud that was passing over the solar modules during that day.
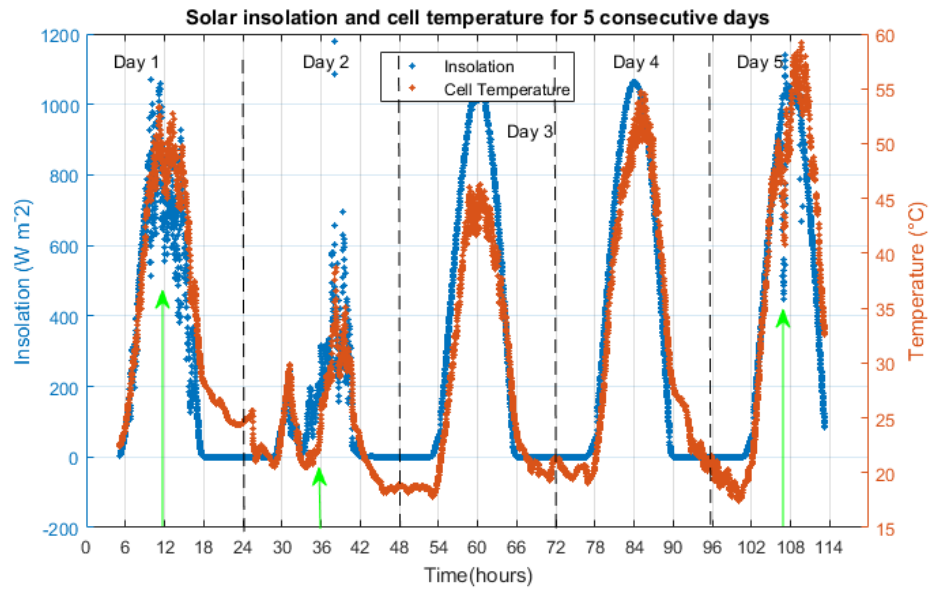

Figure 18: Insolation and cell temperature data for five days (green arrows represent sudden drops in insolation)
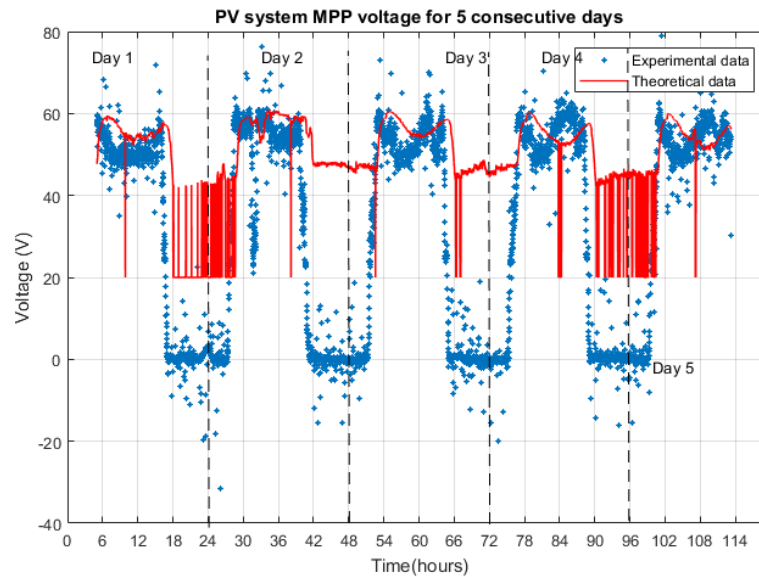

Figure 19: Solar module MPP experimental and theoretical voltage output for five days
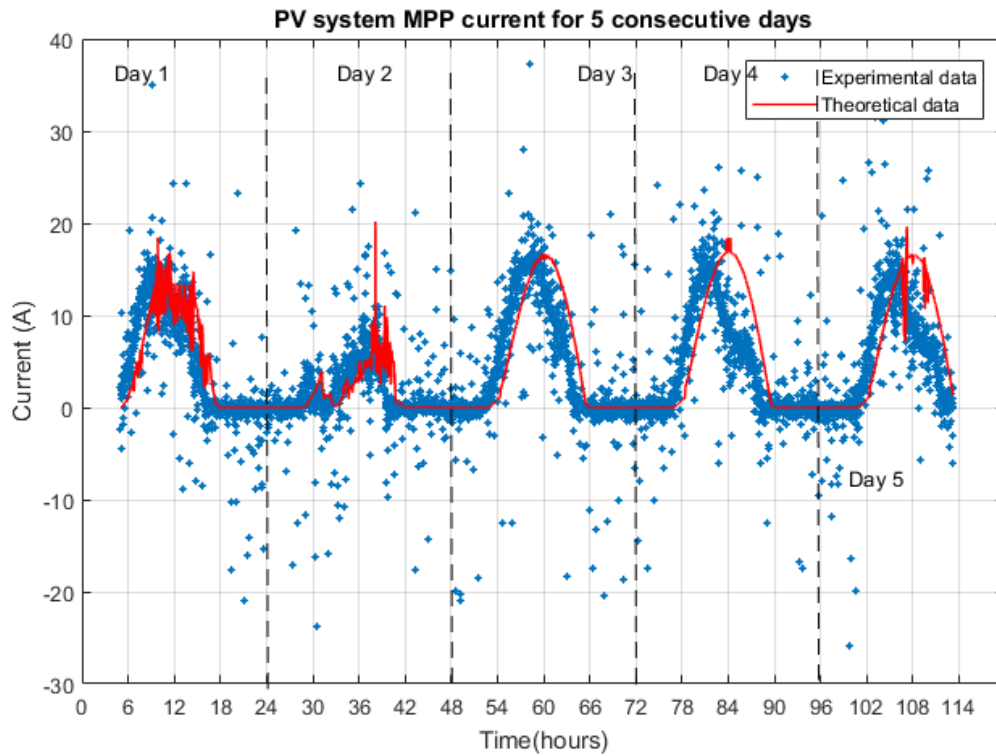
44

Figure 20: Solar module MPP experimental and theoretical current output for five days
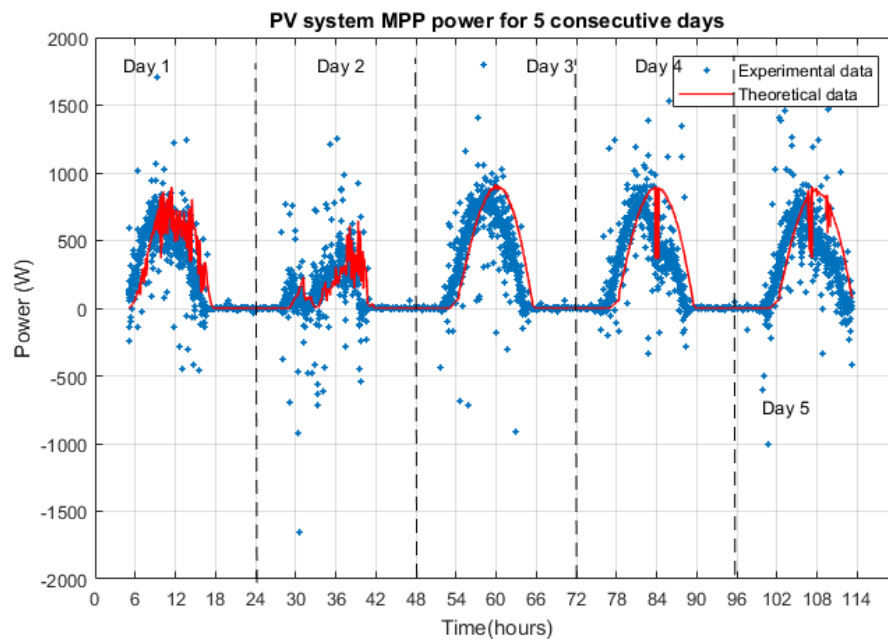

Figure 21: Solar module MPP experimental and theoretical power output for five days

45

Figure 19 shows that solar module model and actual voltage output for the five-day period followed the same trend during day time with some discrepancies to the model's voltage output, which corresponds to sudden drops in insolation values (marked in Figure 18 by green arrows). The solar model perceives those sudden drops in insolation as if an open-circuit occurred in the solar module, which causes the model to produce a voltage value equal to the combined solar module open-circuit voltage (=20 V). At night time when there is no sun (~ after 5 AM), the insolation is ideally 0; however, the insolation sensor gave insulation values below 0 (not physically possible - hard to be observed in Figure 18 due to the negative values being very close to 0) which causes the model to have unexplained ripples in voltage during that time. This is attributed to the fact that model operates when there is sufficient insolation for the solar module operation; hence, its voltage values should not be considered during night time. Moreover, during the night, the experimental curve shows that the solar module produced both positive and negative voltages, which means that the solar module is consuming energy, instead of producing energy. The negative voltages are a common case with the solar module as the electrical potential at the BOS side (battery + MPPT) is higher than the solar module side, forcing current to flow in the reverse direction (reverse current) [60]. The positive voltages is attributed to any artificial source of lighting that may be incident on the solar modules, such as from street light or spotlights.

Figure 20 shows that the solar module current output was able to follow the same path as the experimental current. The experimental curve showed some outliers to the trend which are caused by typical current spikes that occur during solar module operation. As

mentioned above, the negative values in the experimental current curve is a result of the reverse current phenomenon [60]. Similar to the MPP voltage, the experimental current MPP had positive values during the night which is attributed to any source of artificial lighting that maybe incident on the solar modules. Figure 21 shows the experimental and theoretical power output of the solar module calculated by dot multiplying the voltage and current output of each data set and neglecting any negative power output. The model produces a 0 current at night time as expected, which takes cares of the ripples created in the voltage during that time. The experimental and theoretical data energy output for each day from each data set is computed and compared in Table 5. The theoretical energy value was higher than the experimental one since the model did not account for any losses that may occur in the solar module, such as losses in the junction box. The experimental and theoretical values for each day were almost similar with a maximum percentage difference of 17.2 (day 4), which is due to the high number of current spikes that occurred during that day.

Table 5: Daily comparison between the solar module experimental and theoretical energy output

Day	Experimental Energy (kWh)	Theoretical Energy (kWh)	Percentage Difference (%)
1	4.95	5.44	8.96
2	2.23	2.10	6.19
3	5.98	6.75	11.4
4	5.52	6.67	17.2
5	5.34	6.36	16.1
total	24.2	27.3	

Table 6: Total daily sun energy incident on the solar module and theoretical and experimental module efficiency values

Day	Total Sun Energy (kWh)	Module efficiency based on experimental results (%)	Module efficiency based on theoretical results (%)
1	36.2	13.7	15.0
2	13.2	18.4	15.9
3	44.2	13.6	15.9
4	45.8	12.0	14.6
5	43.5	12.3	14.6

To further investigate the solar module model and field-testing results, the power output of the solar modules is compared to the daily Sun's energy input incident on the solar modules, namely the area under the curve of the insolation curve shown in Figure 18 multiplied by the modules total surface area. Table 6 shows the daily sun's energy input and the total efficiency of the solar module system based on the solar energy output values shown in Table 5. The reported manufacturer's module efficiency is 16.3% which is close to the efficiency values presented in Table 6. The slight variation of the module efficiency values from the manufacturer's value is due to partial shading on the solar module that may occur when any shadow hits the surface of the modules, such as the passing of a cloud or a bird.

The analysis presented above shows that the one-diode model was able to accurately predict the solar module power and energy output during the five day period, with a maximum percentage difference of 17.2% between the model and the field-test experimental energy output. Moreover, the module efficiency values based on the model energy output were almost consistent over the 5 day period. Hence, the model's voltage

and current output are reliable to be fed to the FESS to complete the solar-module-FESS system.

8.2. Proposed BLDC bi-directional converter model

As discussed in the Methodology section 7.2, the proposed BLDC bi-directional converter model was implemented as an interface between the solar module system model and the FESS model, as a direct connection between the two independent systems created a non-converging FESS model power and energy output shown in Figures 22-23 respectively. The FESS power output shows a ripple that has a constant increase in magnitude as the day progress, and no clear trend of a sinusoid as expected by the solar module power input. Moreover, the energy accumulation curve of the FESS is in constant increase throughout the day which means the FESS is storing energy at night. This is not physically possible as the only energy source in this system is the solar module which do not produce any energy at night. This is due to the fact that voltage and current input from the solar module is frequently varying, as seen in Figures 19-20. Since the duty cycle of the BLDC model in the FESS is fixed, the FESS cannot handle such rapid variability which causes the power ripples to occur, i.e., the model does not converge to a fixed power value.

Figure 24 shows the proposed model in action with the varying input from the solar module and the corresponding output voltage and current to the FESS based on the duty cycle curve. The proposed model works on minimizing the power loss from the solar module to the FESS (maximize efficiency) while considering all power converter losses to make the proposed model as reliable as possible.

49

In order to force these power ripples to converge to the correct values, the fixed duty cycle is replaced with a varying duty cycle that changes based on the input voltage, which translates to a varying modified FESS impedance from Equation (15) (see section 7.1). The modified load resistance to duty cycle curve is shown in Figure 25. Similar to the solar module validation from the field-testing section above, the analysis on the BLDC bi-directional converter model was performed on a minute-by-minute basis. Hence, every minute, the BLDC model would compute the modified load resistance and based on Figure 25, the duty cycle would change accordingly. The duty cycle decreases as the modified load resistance increases, i.e., when the voltage from the solar module increases, which is due to the nature of buck-boost impedance conversion found in Equation (15).
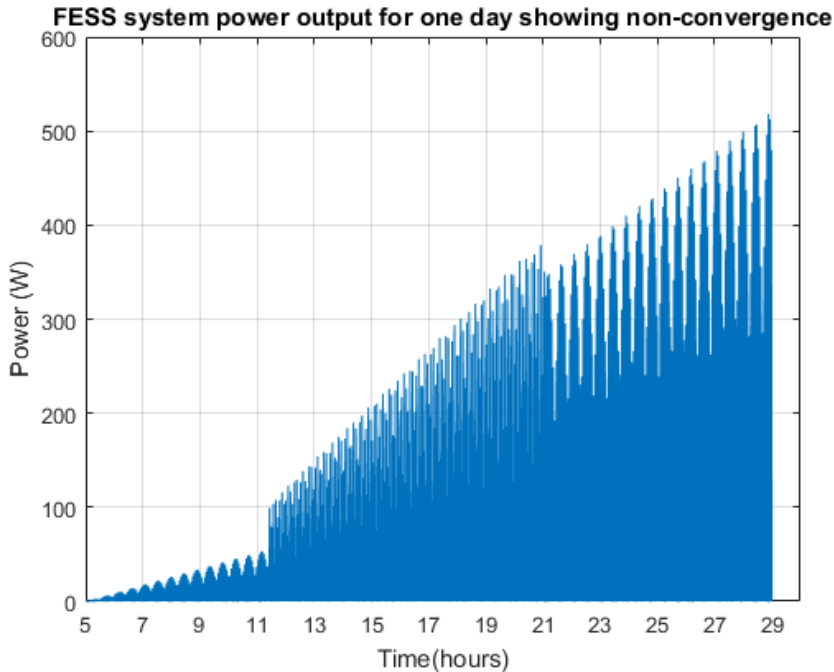
Figure 22: FESS power output without the implementation of the proposed BLDC bi-directional converter model for one day

50
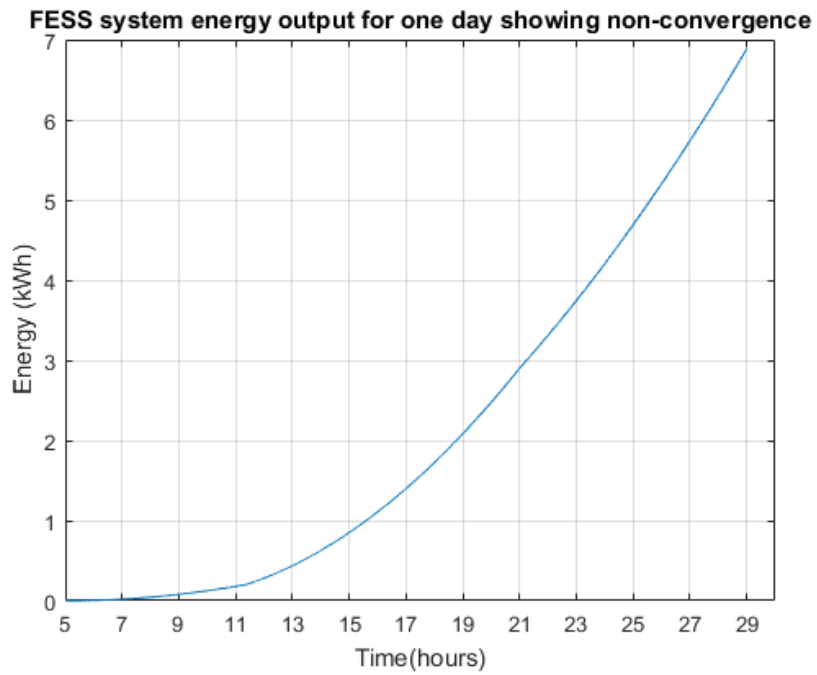
Figure 23: FESS energy output without the implementation of the proposed BLDC bi-directional converter model for one day

Figure 24: BLDC bi-directional converter model input voltage from the solar module and output voltage and current to the FESS

51

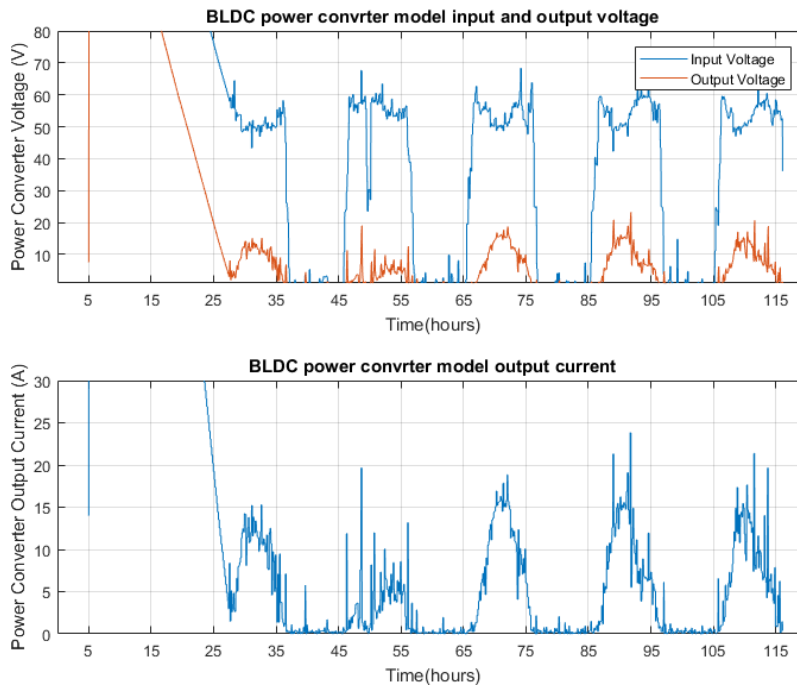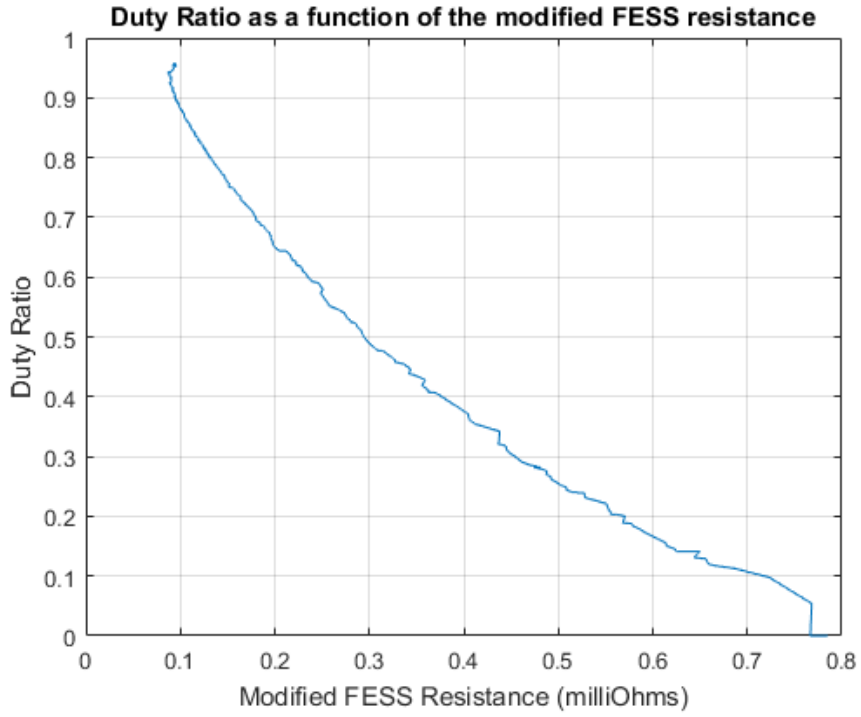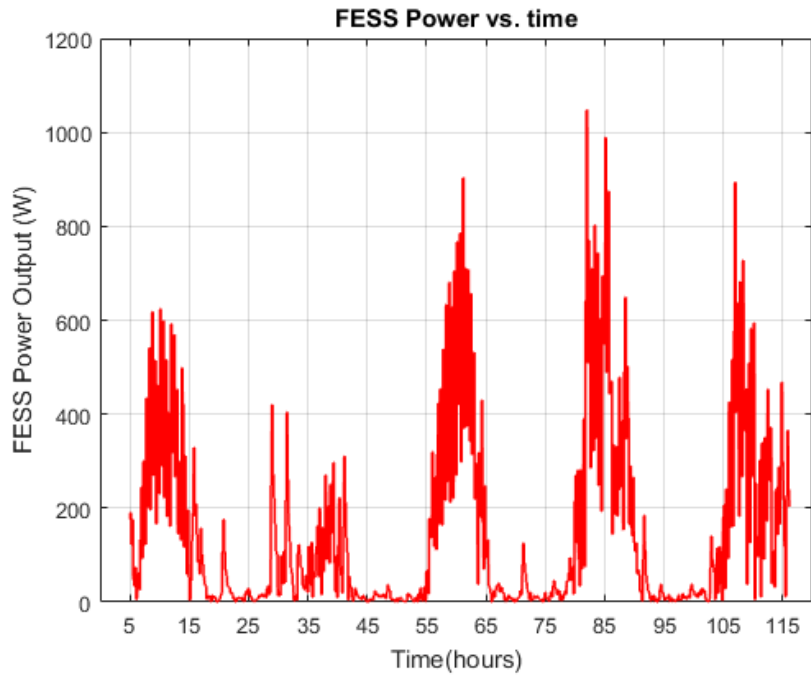Figure 25: Duty ratio selection curve according to the modified load resistance

Figure 26: FESS power showing convergence with the implementation of the proposed BLDC model for five days
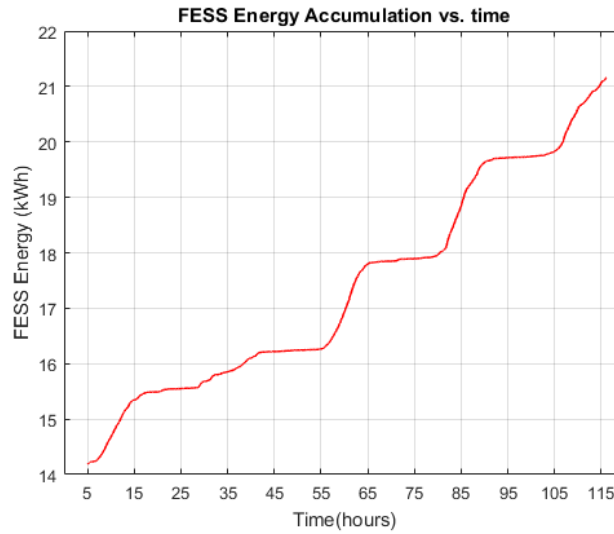
Figure 27: FESS energy showing convergence with the implementation of the proposed BLDC model for five days

The convergence of the FESS after implementing the proposed BLDC bi-directional converter model is outlined in the FESS power and energy output during the five-day period of solar module operation in Figures 26 - 27. The FESS parameters used are outlined in Table 4 in the Methodology section 6.1.2. The FESS power output shows a sinusoid that follows that of the power input from the solar module model, while the energy curve shows that during the night the there is no energy input to the FESS and that the energy output plateaus. Moreover, the FESS energy accumulation over the five-day period reached 21.7 kWh, while the solar module field-test showed that modules produced 24 kWh (Table 5) over the same duration, making the efficiency of the proposed BLDC bi-directional converter model to be 90.4%. Note that the power and energy output do not represent the FESS output in operation, i.e., the charging and discharging schemes of the FESS; it merely shows the convergence of the FESS model using the proposed BLDC bi-directional converter model.

8.3. Representative solar-module-FESS model with load implementation

A load profile was created that represents that of a typical household with a scale that is suitable for the solar module model, i.e., the load profile's energy consumption does not exceed the solar module model energy output [61]. The load profile was then considered in the discharge scheme of the FESS model as the connected load to the bi-directional converter.
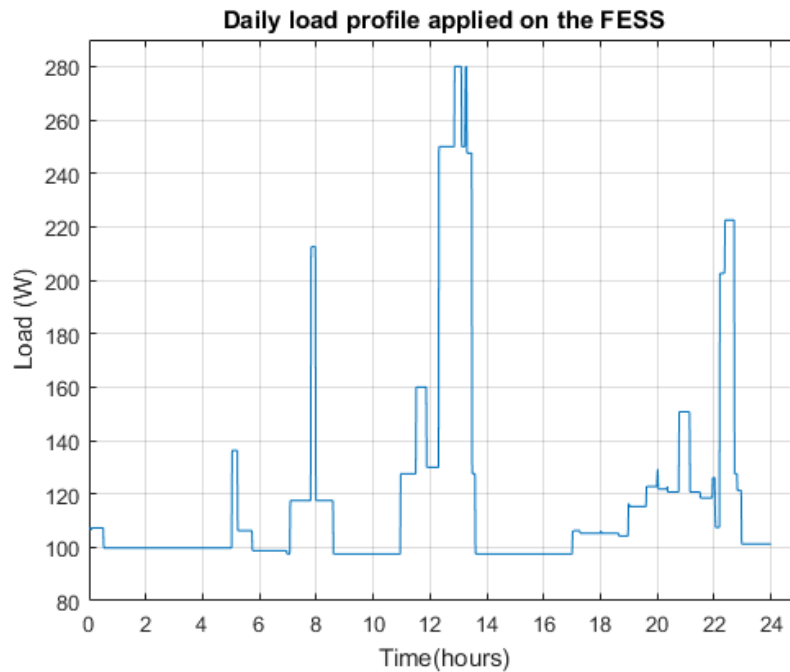

Figure 28: Daily load profile that represents that of a typical household
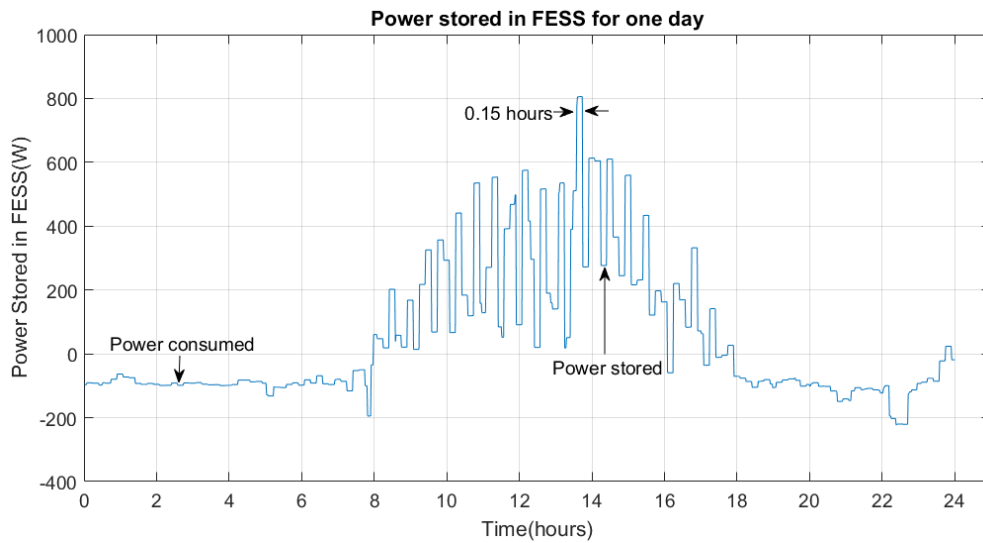
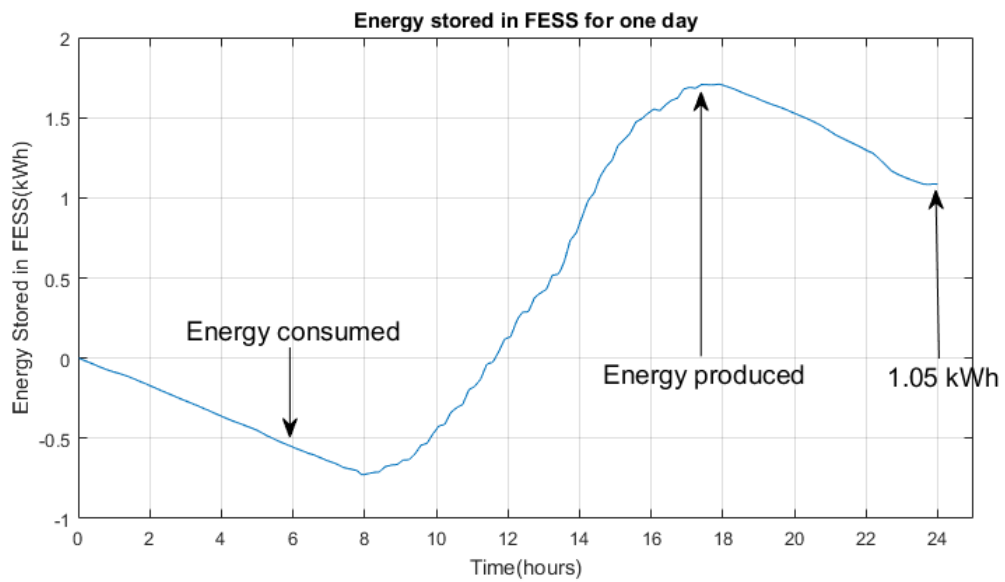Figure 29: Power stored in the FESS throughout the day with applied load

Figure 30: Energy stored in the FESS throughout the day with applied load

Figure 29- 30 present the power and energy stored in the FESS for just one day of solar model operation (day 3). The power of the FESS recorded reached a maximum of 806.2 W at its peak, while the solar module model produced a maximum of 917.8 W maximum. The negative power curve below 0 represents that the solar-module-FESS model is supplying energy to the applied load profile, which typically happens at night time when the solar module model is not supplying any power. At day time, the solar module model is supplying power to the FESS model more than the solar-module-FESS system is supplying power to the applied load; hence, the FESS is storing energy. The accumulated energy in the FESS at any instance during the day is better summarized in Figure 30. Using the load profile shown in Figure 28, the FESS stored an excess of 1.05 kWh at the end of the day, which is available for use to the following day.

The power stored in the FESS shown in Figure 29 follows a ripple trend, which shows a state of frequent charge and discharge patterns that the FESS is going through. One of the advantages of using the FESS as energy storage is the fast charge and discharge duration; hence, the FESS was constantly discharging power to the connected load and then the FESS was recharged in 0.15 hours (=9 minutes).

For the solar-module-FESS model, the solar module energy input is compared with the daily stored energy from the FESS. When comparing the energy outputs from the solar module with the flywheel, a discrepancy of 20.1% was found. The solar module model gave an energy output of 6.75 kWh while the FESS had an output of 5.39 kWh on Day 3 (this is without any application of load to the FESS). This difference in energy outputs can be decreased by considering the inverter and BLDC motor losses. The efficiency of the

designed FESS system to be used in the solar module application is 79.8%, which is higher than the efficiency reported in the literature [62]. The overall solar-module-FESS system efficiency is 11.9%. However, the solar-module-FESS used in literature utilizes different FESS and PV system parameters, such as the dimensions of the flywheel, motor constants of the BLDC motor, and overall voltage and current output of the PV system. Hence, any comparison with other literature requires that both systems need to be of the same sizing.
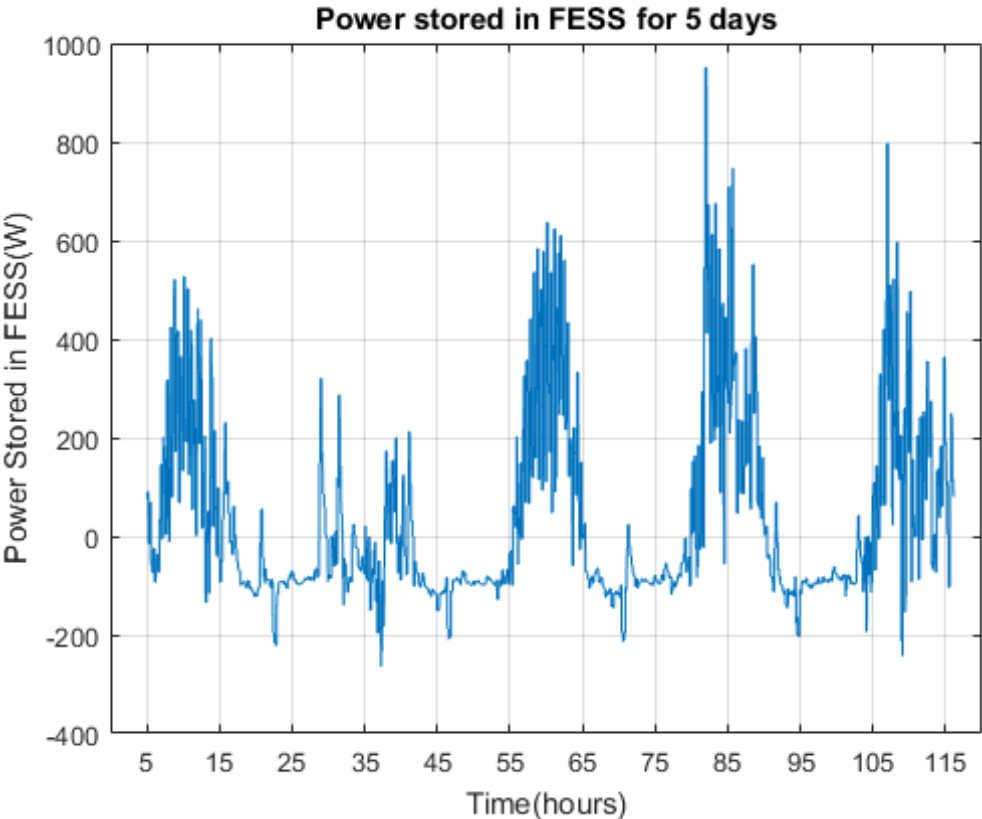

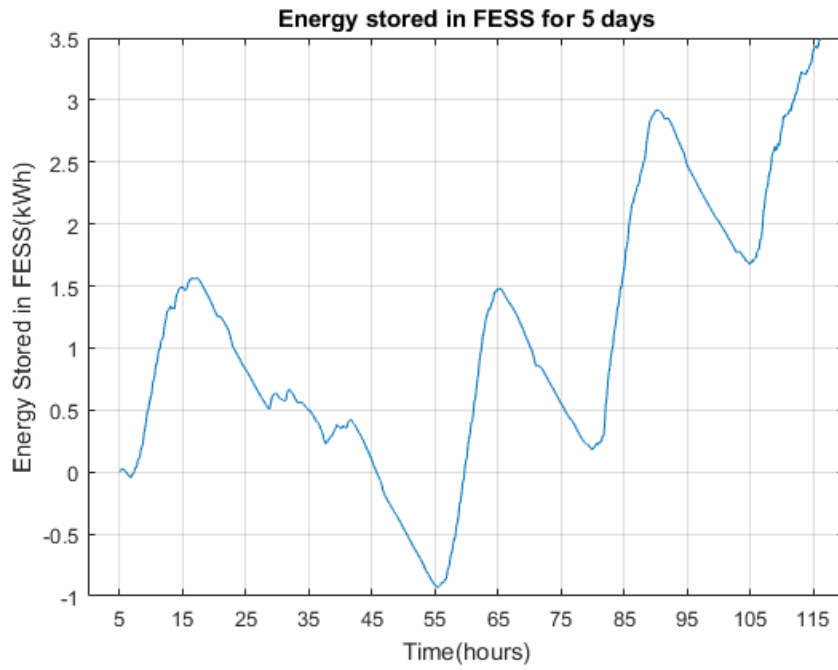Figure 31: Power stored in the FESS throughout the 5 days with applied load

Figure 32: Energy stored in the FESS throughout the 5 days with applied load
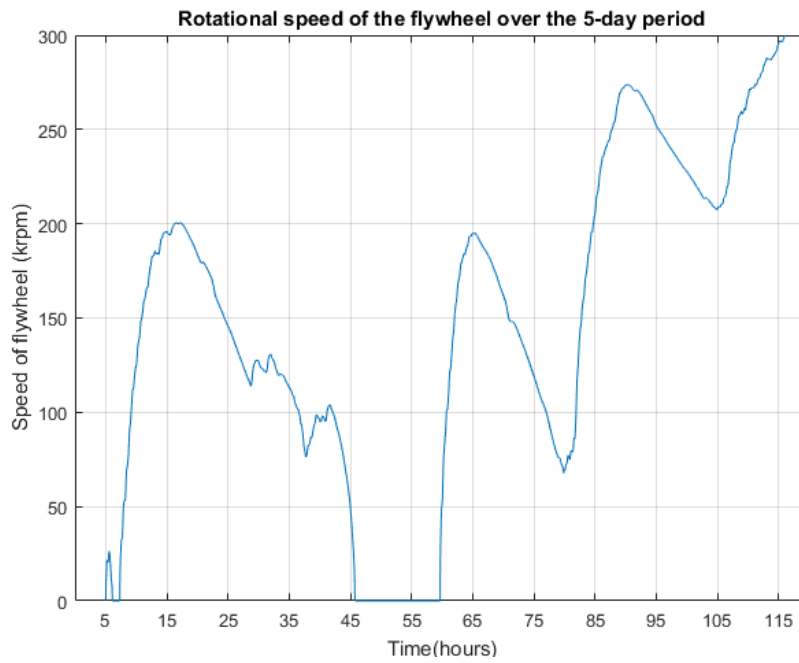

Figure 33: Rotational speed of the flywheel showing that it stalls (speed = 0) when the energy stored was negative, and reaches the maximum speed of 300 krpm after the 5 days

58

The FESS power, energy, and flywheel rotational speed using the charge and discharge schemes for the 5 days are shown in Figures 31 - 33. As shown in Figure 31, the start of the simulation (start of Day 1) initiated at day time (5 AM) as to let the FESS have some initial stored energy; however, the charge from Day 1 into the FESS was not sufficient for Day 2, and the energy stored in the FESS was below zero after Day 2 was finished. This means that the FESS will not be able to supply any power to the load. This is attributed to the fact that the solar module model did not produce enough energy in Day 2 due to insufficient solar insolation on that day, which is evident in the insolation curve, and the theoretical solar module power output curve (Figure 18 and 21). As a result, the flywheel stalls and its rotational speed drops to 0. Such difficulties are often experienced in solar applications, where the power output of the solar module could be reduced significantly due to forces of nature, such as the passing of a cloud, or a bird, on part (partial shading) or the entirety of the solar module (complete shading). A solution to such difficulties is to install a smaller backup solar module which is placed on a different part of the roof of TAMUQ, and connected to the FESS; however, this adds to the cost and bulkiness of the overall solar-module-FESS setup. Nevertheless, due to the abundant solar insolation present on the following days, the energy stored in the FESS continued to be in excess, until reaching a total excess of 3.51 kWh at the end of the five days and the flywheel reached its maximum speed of 300 krpm. All in all, the solar-module-FESS system model was able to predict the overall system output and can be used on other solar module systems and FESS units in a timely-effective fashion.

9. CONCLUSION, CONTRIBUTION AND FUTURE WORK

This section details the current and future additions of this project to the field of research of photovoltaic (PV) systems associated with Flywheel Energy Storage Systems (FESS).

9.1. Conclusion

The ever-increasing solar energy production, characterized by its self-sustainability and environment friendliness, has drastically increased the demand for efficient solar energy storage systems (ESS). The purpose of the ESS is to save the solar energy at times where the energy is plentiful and provide energy to a load at times when the energy is lacking. Commercially available ESS are mainly lead-acid batteries, which has a limited lifetime of two years and a limited efficiency of 60% or less, as well as associated negative environmental impacts . An alternative ESS solution is the Flywheel energy storage systems (FESS) which have merits of high efficiency, long life, and environmental friendliness. However, the intermittences and fluctuations associated to the photovoltaic power (PV) have always acted as a hindrance for the FESS to act as efficient energy storages to the solar module (reported maximum of 40% efficiency [63]). Various research provides methods for the FESS to regulate the power output of the PV system while optimizing the harnessed solar energy; however, limited papers quantify the efficiency and reliability of the FESS in completing such task. Moreover, there is no commercially available FESS for off-grid or residential PV systems.

This research presents proposing a bi-directional converter that acts as an efficient interface between the solar module system and the FESS unit. The solar module system and the FESS have been mathematically modeled and implemented on an open-source MATLAB/SIMULINK platform. The solar model predicts the daily solar power and energy output, which was verified by the solar module system designed and installed on the roof of the TAMUQ building. The parameters of the FESS model were chosen based on the manufacturer data of a high-speed slot-less Brushless DC (BLDC) motor used in a FESS under development. The connected load on the combined solar-module-FESS system was modeled based on a typical load profile of a household. The load profile was scaled down to accommodate the power rating of the BLDC motor-generator (MG) driving the FESS. The proposed bi-directional converter was mathematically modeled and incorporated in the BLDC compartment of the FESS model. The converter model regulated the solar module model fluctuations through implementing a varying duty cycle (instead of the typical fixed duty cycle). The duty cycle is altered based on the solar model voltage and current, which translates to a varying modified FESS model impedance. The modified solar-module-FESS simulation was performed during a five-day period, with a sample period of 1 minute. The average efficiency of the solar module model (defined as the daily solar module energy output divided by the total daily insolation incident on the solar modules surface area) was 15%, with an average percentage difference of 12% between the simulated and the measured energy output. The efficiency of the FESS model was 79.8% which was higher than both the reported efficiency of lead-acid batteries (60%) and FESS (40%) in off-grid PV systems. The speed of the flywheel model was calculated

61

using the resulting FESS energy output; the maximum flywheel speed reached a maximum of 300 krpm, which is in accord with the calculated by provided by the manufacturer. The proposed bi-directional converter model enables the FESS to be commercially available and to be an efficient energy storage solution for low-power off-grid PV systems such as a residential PV power source.

9.2. Contribution

Even though the standalone FESS is more efficient than batteries (Table 1); however, the PV intermittences and fluctuations have caused the FESS to have a lower efficiency than batteries in energy storage for PV applications. Thus, the contribution of this research to the field is:

- Developed a mathematical interface model that can regulate the power output of the PV system while optimizing the solar energy for the FESS. The interface model is implemented in the power electronics of the motor-generator (MG) electrical machine driving the FESS.

- The developed interface model enables the FESS to store energy from a residential solar module system with an efficiency of 79.8%, which is higher than the efficiency of the FESS model developed for a residential PV system conducted in [63] (40% efficiency).

- The developed interface model enables the FESS to be a commercially available and an efficient energy storage solution for low-power off-grid PV systems such as a residential PV power source. There is no commercially available FESS for off-grid or residential PV systems [63].

- The modified FESS model (FESS + interface model) output is in accord with the solar module input, and the solar-module-FESS system overall efficiency values match those provided in literature. Hence, the novel interface model is verified and can be used to interface between PV applications and FESS (BLDC type) of different architecture and parameters.

9.3. Future work

The research presented a mathematical model for the combined solar-module-FESS system with an efficiency that surpasses the efficiency of the FESS presented in literature; however, there are some recommendations that can be implemented on the combined model to improve its reliability and its representativeness to a real-life system:

- Use a double-diode instead of a single-diode solar cell circuit to model the solar module system. The double-diode mathematical model yields a more accurate solar module power output than the single-diode one; however, there are a higher number of unknowns in the double-diode model, which increases the computational time.

- Use a higher number (12 instead of 6) of metal oxide semiconductor field-effect transistors (MOSFETs) and insulate gate bipolar transistors (IGBTs) in the BLDC bi-directional converter model. The higher number of transistors is capable of producing a voltage and current operating point that is more efficient for the FESS to operate at, which is not able to be achieved at a lower number of transistors.

- Incorporate the fact that an ideal vacuum situation cannot be achieved in the FESS containment chamber, and introduce to the FESS model a viscous drag force that is proportional to the speed of the flywheel.

- Expand the FESS model to incorporate different FESS motor-generator options other than the BLDC, such as an induction machine or a variable reluctant machine (VRM).

REFERENCES

[1] Singh, O., and Rajput, S. K., "Mathematical modelling and simulation of solar photovoltaic array system," Proc. Research Advances in Integrated Navigation Systems (RAINS), International Conference on, IEEE, pp. 1-5.

[2] Fraas, L. M., 2014, "History of solar cell development," Low-Cost Solar Electric Power, Springer, pp. 1-12.

[3] Schmela, M., 2019, "Global Market Outlook 2019 - 2023," last modified May 10, 2019, accessed July 19, 2019, https://www.solarpowereurope.org/global-market-outlook-2019-2023/.

[4] Ferrari, S., Lazzaroni, M., Piuri, V., Salman, A., Cristaldi, L., Faifer, M., and Toscani, S., 2016, "Solar panel modelling through computational intelligence techniques," Measurement, 93, pp. 572-580.

[5] Del Canizo, C., Del Coso, G., and Sinke, W., 2009, "Crystalline silicon solar module technology: Towards the 1€ per watt-peak goal," Progress in Photovoltaics: Research and Applications, 17(3), pp. 199-209.

[6] Makrides, G., Zinsser, B., Norton, M., Georghiou, G. E., Schubert, M., and Werner, J. H., 2010, "Potential of photovoltaic systems in countries with high solar irradiation," Renewable and Sustainable Energy Reviews, 14(2), pp. 754-762.

[7] Messenger, R. A., and Abtahi, A., 2010, "Introduction to PV Systems," Photovoltaic Systems Engineering, C. Press, ed., CRC press, London, New York, p. 85.

[8] Goetzberger, A., Knobloch, J., and Voss, B., 1998, "Crystalline silicon solar cells," New York, pp. 114-118.

[9] Ferrari, S., Lazzaroni, M., Piuri, V., Salman, A., Cristaldi, L., Faifer, M., and Toscani, S., "A computational intelligence approach to solar panel modelling," Proc. Instrumentation and Measurement Technology Conference (I2MTC) Proceedings, 2014 IEEE International, IEEE, pp. 1261-1266.

[10] Chiu, C.-S., and Ouyang, Y.-L., 2011, "Robust maximum power tracking control of uncertain photovoltaic systems: A unified TS fuzzy model-based approach," IEEE Transactions on Control Systems Technology, 19(6), pp. 1516-1526.

[11] Esram, T., and Chapman, P. L., 2007, "Comparison of photovoltaic array maximum power point tracking techniques," IEEE Transactions on Energy Conversion, 22(2), pp. 439-449.

[12] Kottas, T. L., Boutalis, Y. S., and Karlis, A. D., 2006, "New maximum power point tracker for PV arrays using fuzzy controller in close cooperation with fuzzy cognitive networks," IEEE Transactions on Energy Conversion, 21(3), pp. 793-803.

[13] Mirecki, A., Roboam, X., and Richardeau, F., "Comparative study of maximum power strategy in wind turbines," Proc. Industrial Electronics, 2004 IEEE International Symposium on, IEEE, pp. 993-998.

[14] Jossen, A., Garche, J., and Sauer, D. U., 2004, "Operation conditions of batteries in PV applications," Solar Energy, 76(6), pp. 759-769.

[15] Amiryar, M., and Pullen, K., 2017, "A review of flywheel energy storage system technologies and their applications," Applied Sciences, 7(3), p. 286.

[16] Bolund, B., Bernhoff, H., and Leijon, M., 2007, "Flywheel energy and power storage systems," Renewable and Sustainable Energy Reviews, 11(2), pp. 235-258.

[17] Sebastián, R., and Alzola, R. P., 2012, "Flywheel energy storage systems: Review and simulation for an isolated wind power system," Renewable and Sustainable Energy Reviews, 16(9), pp. 6803-6813.

[18] Pena-Alzola, R., Campos-Gaona, D., and Ordonez, M., "Control of flywheel energy storage systems as virtual synchronous machines for microgrids," Proc. 2015 IEEE 16th Workshop on Control and Modeling for Power Electronics (COMPEL), IEEE, pp. 1-7.

[19] Hebner, R., Beno, J., and Walls, A., 2002, "Flywheel batteries come around again," IEEE Spectrum, 39(4), pp. 46-51.

[20] Liu, H., and Jiang, J., 2007, "Flywheel energy storage—An upswing technology for energy sustainability," Energy and Buildings, 39(5), pp. 599-604.

[21] Chen, H., Cong, T. N., Yang, W., Tan, C., Li, Y., and Ding, Y., 2009, "Progress in electrical energy storage system: A critical review," Progress in Natural Science, 19(3), pp. 291-312.

[22] Cimuca, G. O., Saudemont, C., Robyns, B., and Radulescu, M. M., 2006, "Control and performance evaluation of a flywheel energy-storage system associated to a variable-speed wind generator," IEEE Transactions on Industrial Electronics, 53(4), pp. 1074-1085.

[23] Ye, S., and Sun, B., "Application of flywheel battery in solar power system," Proc. 2009 International Conference on Energy and Environment Technology, IEEE, pp. 533-536.

[24] Sadiq, M., 2018, "Solar water heating system for residential consumers of Islamabad, Pakistan: A cost benefit analysis," Journal of Cleaner Production, 172, pp. 2443-2453.

[25] Ibrahim, H., Ilinca, A., and Perron, J., 2008, "Energy storage systems—Characteristics and comparisons," Renewable and Sustainable Energy Reviews, 12(5), pp. 1221-1250.

[26] Panwar, N., Kaushik, S., and Kothari, S., 2011, "Role of renewable energy sources in environmental protection: a review," Renewable and Sustainable Energy Reviews, 15(3), pp. 1513-1524.

[27] Shao, Q., Zhao, Y., Du, S., Du, Y., Lee, W. Y., Kim, T. M., Kim, M. J., Ko, Y., and Kim, J. D., 2016, "A novel hybrid energy storage strategy based on flywheel and lead-acid battery in wind power generation system," International Journal of Control and Automation, 8(7), pp. 1-12.

[28] Nguyen, X. H., and Nguyen, M. P., 2015, "Mathematical modeling of photovoltaic cell/module/arrays with tags in Matlab/Simulink," Environmental Systems Research, 4(1), p. 24.

[29] Dehghanzadeh, A., Farahani, G., and Maboodi, M., 2017, "A novel approximate explicit double-diode model of solar cells for use in simulation studies," Renewable Energy, 103, pp. 468-477.

[30] Tamrakar, V., Gupta, S., and Sawle, Y., 2015, "Single-Diode PV Cell modeling and study of characteristics of single and two-diode equivalent circuit," Electrical and Electronics Engineering: An International Journal (ELELIJ), 4(3), pp. 13-24.

[31] Ishaque, K., and Salam, Z., 2011, "A comprehensive MATLAB Simulink PV system simulator with partial shading capability based on two-diode model," Solar Energy, 85(9), pp. 2217-2227.

[32] Shannan, N. M. A. A., Yahaya, N. Z., and Singh, B., "Single-diode model and two-diode model of PV modules: A comparison," Proc. 2013 IEEE International Conference on Control System, Computing and Engineering, IEEE, pp. 210-214.

[33] Ismail, M. S., Moghavvemi, M., and Mahlia, T., 2013, "Characterization of PV panel and global optimization of its model parameters using genetic algorithm," Energy Conversion and Management, 73, pp. 10-25.

[34] Villalva, M. G., Gazoli, J. R., and Ruppert Filho, E., "Modeling and circuit-based simulation of photovoltaic arrays," Proc. 2009 Brazilian Power Electronics Conference, IEEE, pp. 1244-1254.

[35] Kanimozhi, G., and Kumar, H., 2018, "Modeling of solar cell under different conditions by Ant Lion Optimizer with LambertW function," Applied Soft Computing, 71, pp. 141-151.

[36] Park, J.-Y., and Choi, S.-J., 2017, "A novel simulation model for PV panels based on datasheet parameter tuning," Solar Energy, 145, pp. 90-98.

[37] Ahmed, C. B., Kassas, M., and Ahmed, S. E., "LabVIEW Based PV Panel Online Characteristics and Parameters Estimation," Proc. ANT/SEIT, pp. 876-882.

[38] Benmessaoud, M., Boudghene Stambouli, A., Midoun, A., Zegrar, M., Zerhouni, F., and Zerhouni, M., 2010, "Proposed methods to increase the output efficiency of a photovoltaic (PV) system," Acta Polytech. Hung, 7(2), p. 11.

[39] Chenni, R., Makhlouf, M., Kerbache, T., and Bouzid, A., 2007, "A detailed modeling method for photovoltaic cells," Energy, 32(9), pp. 1724-1730.

[40] Walker, G., 2001, "Evaluating MPPT converter topologies using a MATLAB PV model," Journal of Electrical & Electronics Engineering, Australia, 21(1), p. 49.

[41] Bellia, H., Youcef, R., and Fatima, M., 2014, "A detailed modeling of photovoltaic module using MATLAB," NRIAG Journal of Astronomy and Geophysics, 3(1), pp. 53-61.

[42] Chouder, A., Silvestre, S., Sadaoui, N., and Rahmani, L., 2012, "Modeling and simulation of a grid connected PV system based on the evaluation of main PV module parameters," Simulation Modelling Practice and Theory, 20(1), pp. 46-58.

[43] Shiau, J.-K., Lee, M.-Y., Wei, Y.-C., and Chen, B.-C., 2014, "Circuit simulation for solar power maximum power point tracking with different buck-boost converter topologies," Energies, 7(8), pp. 5027-5046.

[44] Cubas, J., Pindado, S., and De Manuel, C., 2014, "Explicit expressions for solar panel equivalent circuit parameters based on analytical formulation and the Lambert W-function," Energies, 7(7), pp. 4098-4115.

[45] MathWorks, I., 2015, MATLAB : SIMSCAPE Power Systems Specialized Technology Renewable Energy Block Library, Hydro-Quebec and The Math Works Inc., 2015.

[46] Pena-Alzola, R., Sebastián, R., Quesada, J., and Colmenar, A., "Review of flywheel based energy storage systems," Proc. 2011 International Conference on Power Engineering, Energy and Electrical Drives, IEEE, pp. 1-6.

[47] Samineni, S., Johnson, B. K., Hess, H. L., and Law, J. D., "Modeling and analysis of a flywheel energy storage system with a power converter interface," Proc. International Conference on Power Systems Transients (IPST), New Orleans, USA.

[48] Gonçalves de Oliveira, J., 2011, "Power control systems in a flywheel based all-electric driveline," Acta Universitatis Upsaliensis.

[49] Arghandeh, R., Pipattanasomporn, M., and Rahman, S., 2012, "Flywheel energy storage systems for ride-through applications in a facility microgrid," IEEE Transactions on Smart Grid, 3(4), pp. 1955-1962.

[50] Siostrzonek, T., Penczek, A., and Pirog, S., "The control and structure of the power electronic system supplying the flywheel energy storage (FES)," Proc. 2007 European Conference on Power Electronics and Applications, IEEE, pp. 1-8.

[51] Su, W., Jin, T., and Wang, S., "Modeling and simulation of short-term energy storage: Flywheel," Proc. 2010 International Conference on Advances in Energy Engineering, IEEE, pp. 9-12.

[52] Östergård, R., 2011, "Flywheel energy storage: a conceptucal study."

[53] Chin, Y.-K. R., and Soulard, J., 2003, "Modeling of iron losses in permanent magnet synchronous motors with field-weakening capability for electric vehicles," International Journal of Automotive Technology, 4(2), pp. 87-94.

[54] Eckroad, S., 1999, "Flywheels for electric utility energy storage," Technical Report. Electric Power Research Institute, Palo Alto, CA, EPRI ….

[55] MathWorks, I., 2013, MATLAB : SIMSCAPE Electrical Power Systems, The Math Works Inc., 2013.

[56] Bozorgi, A. M., Fereshtehpoor, V., Monfared, M., and Namjoo, N., 2015, "Controller Design Using Ant Colony Algorithm for a Non-inverting Buck–Boost Chopper Based on a Detailed Average Model," Electric Power Components and Systems, 43(2), pp. 177-188.

[57] Sayed, K., Abdel-Salam, M., Ahmed, A., and Ahmed, M., 2012, "New high voltage gain dual-boost DC-DC converter for photovoltaic power systems," Electric Power Components and Systems, 40(7), pp. 711-728.

[58] Xiao, H., and Xie, S., 2012, "Interleaving double-switch buck–boost converter," IET Power Electronics, 5(6), pp. 899-908.

[59] MathWorks, I., 2019, MATLAB : SIMSCAPE Electrical Buck Boost Converter, The Math Works Inc., 2019.

[60] Zhao, Y., Lehman, B., DePalma, J.-F., Mosesian, J., and Lyons, R., "Fault evolution in photovoltaic array during night-to-day transition," Proc. 2010 IEEE 12th workshop on control and modeling for power electronics (COMPEL), IEEE, pp. 1-6.

[61] Mohamed, M. T., 2018, "Completely Off-grid PV System Design for a Qatari Household," Report.

[62] Cimuca, G., Radulescu, M. M., Saudemont, C., and Robyns, B., "Losses and Efficiency of a Flywheel Energy Storage System with Permanent-Magnet Synchronous Machine Associated to a Variable-Speed Wind Generator," Proc. ICEM 2004.

[63] Li, X., Erd, N., and Binder, A., "Evaluation of flywheel energy storage systems for residential photovoltaic installations," Proc. 2016 International Symposium on Power Electronics, Electrical Drives, Automation and Motion (SPEEDAM), IEEE, pp. 255-260.